A COMPARATIVE ANALYSIS OF GEOREFERENCING TECHNIQUES FOR CROP CANOPY HEIGHT ESTIMATION USING UAS PHOTOGRAMMETRY

A Thesis

by

JOSE LUIS LANDIVAR SCOTT

B.S. University of Arkansas, 2020

Submitted in Partial Fulfillment of the Requirements for the Degree of

MASTER OF SCIENCE

in

GEOSPATIAL SYSTEMS ENGINEERING

Texas A&M University-Corpus Christi
Corpus Christi, Texas

August 2023

A COMPARATIVE ANALYSIS OF GEOREFERENCING TECHNIQUES FOR CROP CANOPY HEIGHT ESTIMATION USING UAS PHOTOGRAMMETRY

A Thesis

by

JOSE LUIS LANDIVAR SCOTT

This thesis meets the standards for scope and quality of
Texas A&M University-Corpus Christi and is hereby approved.

Michael J. Starek, PhD
Chair

Mahendra Bhandari, PhD
Co-Chair

Tianxing Chu, PhD
Committee Member

August 2023

ABSTRACT

In the rapidly evolving fields of geospatial engineering and precision agriculture, the accuracy and reliability of georeferencing techniques and Uncrewed Aircraft System (UAS) methodologies are crucial for effective decision-making and crop management. This research aims to enhance UAS Structure-from-Motion (SfM) photogrammetry data quality for crop canopy height estimation in high-throughput phenotyping. The study investigates and compares the accuracy and reliability of three distinct methods used for georeferencing of the UAS imagery, which subsequently enables more accurate SfM 3D reconstruction: Global Navigation Satellite System (GNSS) without any correction aiding (GNSS-only), GNSS+Real-Time Kinematic (RTK), receiving RTK corrections from a local base station, GNSS+Real-Time Network (RTN), receiving RTK corrections from the Texas Department of Transportation (TxDOT) GNSS reference station network. The study further assesses the correlation between manually measured plant heights and those estimated from UAS-SfM point cloud data, exploring three different Digital Terrain Model (DTM) generation techniques.

The research was conducted at the Texas A&M AgriLife Research and Extension Center in Corpus Christi, Texas, USA, on corn crops grown during the 2022 agricultural season. The three DTM generation methods under consideration included 1) using a DTM acquired from a flight conducted before plant emergence, 2) creating a DTM by interpolating ground height points, and 3) implementing automatic classification algorithms.

Findings initially revealed that the GNSS+RTK method consistently outperformed the other georeferencing techniques, delivering more accurate results across various dates. Despite these overall trends, there were some instances where the GNSS+RTK method did not consistently outperform the other techniques. The use of one ground control point (GCP) improved georeferencing accuracy compared to scenarios with no GCPs used, while GNSS-only without correction aiding reported the least accurate results as expected. Regarding plant height estimation, the highest accuracy was generally achieved with greater canopy cover percentages, with the optimal percentage vary-ing depending on the data collection date and DTM creation method. The highest coefficient of determination (R^2) of 0.92 between manual measurements and UAS-SfM derived plant heights was found when the DTM was either interpolated from ground height points or obtained from a pre-emergence flight.

DEDICATION

This work is completely dedicated to my respectful parents and to my institution mentors under whose constant guidance I have completed this thesis. They not only enlightened me with academic knowledge but also gave me valuable advice whenever I needed it the most.

ACKNOWLEDGEMENTS

I would like to express my deepest gratitude to my honorable supervisor, Dr. Michael Starek, for his invaluable supervision, support, and tutorship throughout the course of my Master's degree. I am profoundly grateful to the Faculty of Texas A&M AgriLife Research for providing the funding opportunity that enabled me to undertake my studies at the Department of College of Science and Engineering, Texas A&M University-Corpus Christi.

Additionally, I would like to extend my sincere appreciation to Dr. Mahendra Bhandari for his treasured support, which played a crucial role in shaping my experimental methods. I am also grateful to Dr. Juan Landivar and Dr. Tianxing Chu for their mentorship during this journey.

I would like to acknowledge my friends, colleagues, and research team – Daniela Urbano, Francisco M. Gaona, Harsha Vardhan, and Sindhu Priya – for the cherished time spent together in the lab and social settings, which made this experience truly memorable.

Finally, my heartfelt appreciation goes out to my family and friends for their inexhaustible encouragement and support throughout my studies. This accomplishment would not have been possible without their love and belief in me.

TABLE OF CONTENTS

Page

ABSTRACT iv

DEDICATION vi

ACKNOWLEDGEMENTS vii

TABLE OF CONTENTS viii

LIST OF FIGURES xi

LIST OF TABLES xii

CHAPTER 1: INTRODUCTION 1

1.1 Motivation 1

1.2 Background 2

1.3 Objectives 4

CHAPTER 2: REVIEW OF THE LITERATURE 5

2.1 Precision Agriculture 5

2.1.1 Advancements in UAS technology for agricultural applications 6

2.2 Remote Sensing for Precision Agriculture 7

2.2.1 UAS Approaches 7

2.3 Structure-from-Motion Phtogrammetry 8

2.3.1 Georeferencing methods for UAS-SfM 11

2.3.1.1 GNSS+RTK 12

2.3.1.2 GNSS+RTN 13

2.3.1.3 GNSS+PPK 13

2.3.1.4 GNSS+PPP 14

2.3.1.5 Standalone GNSS 14

2.3.1.6 Comparison of accuracy and efficiency 15

2.4 UAS SfM & LiDAR for Crop Height Monitoring 16

2.4.1 UAS-SfM for Crop Height Monitoring 16

2.4.2 UAS-LiDAR for Crop Height Monitoring 17
2.5 DTM Generation Techniques 18
2.5.1 DTM obtained from a pre-plant emergence flight 18
2.5.2 DTM based on interpolating ground height points 18
2.5.3 DTM created using automatic classification algorithms in PIX4Dmapper 18
2.5.4 Comparison of accuracy and reliability 19
CHAPTER 3: MATERIALS & METHODS 20
3.1 Study Location 20
3.2 Equipment & Tools 21
3.2.1 UAS Platform & GNSS receiver 21
3.2.2 PIX4Dmapper & QGIS 25
3.3 Data Collection 26
3.3.1 UAS Flights 26
3.3.2 Field Measurements 27
CHAPTER 4: METHODOLOGY 29
4.1 Georeferencing Systems Comparison 29
4.1.1 Standalone GNSS 31
4.1.2 GNSS+RTK 31
4.1.3 GNSS+RTN 32
4.2 Plant Height Estimation 33
4.3 SfM Data Processing 33
4.3.1 Georeferencing Studies 34
4.3.1.1 Import Imagery 34
4.3.1.2 Photo Alignment & Calibration 34
4.3.1.3 Import GCPs & Re-optimize 35
4.3.1.4 Generate Quality Report 36
4.3.2 Plant Height Studies 36

4.3.2.1 Import Imagery 36
4.3.2.2 Photo Alignment & Calibration 37
4.3.2.3 Import GCPs & Re-optimize 37
4.3.2.4 Point Cloud and Mesh 38
4.3.2.5 Generate DSM, DTM, and Orthomosaic 38
4.3.3 Generate CHM 39
4.3.4 Obtain Plant Height 39
4.3.5 Generate Canopy Cover 39
4.4 Comparative Accuracy Assessment 40
4.5 Estimating Plant Height from SfM 41
4.5.1 Statistical Evaluation of UAS-SfM Plant Height Estimation Error 43
CHAPTER 5: RESULTS & DISCUSSION 44
5.1 Georeferencing Systems Comparison 44
5.1.1 Results 44
5.1.2 Discussion 55
5.2 Plant Height Estimation 56
5.2.1 Results 56
5.2.2 Discussion 59
CHAPTER 6: CONCLUSIONS & FUTURE WORK 61
6.1 Conclusions 61
6.2 Recommendations & Future Work 62
REFERENCES 64

LIST OF FIGURES

		Page
2.1	Structure from Motion (SfM) workflow	10
3.2	Study Area	21
3.3	Hardware utilized	22
3.4	Texas Department of Transportation (TxDOT) Real-Time Network (RTN)	24
3.5	Illustration of a corn plant	28
4.6	Graphical representation of different positioning systems	29
4.7	Ground Control Points (GCPs) distribution for georeferencing study	30
4.8	Ground Control Points (GCPs) distribution for plant height study	33
4.9	Illustration of the UAS green canopy cover estimation workflow	40
4.10	Checkpoint georeferencing errors	41
4.11	Illustration of the UAS derived plant height estimation workflow	42
4.12	Schematic representation of plot boundaries	43
5.13	Horizontal Accuracy Assessment (X) - 20220601	44
5.14	Horizontal Accuracy Assessment (Y) - 20220601	45
5.15	Vertical Accuracy Assessment (Z) - 20220601	45
5.16	Horizontal Accuracy Assessment (X) - 20220616	46
5.17	Horizontal Accuracy Assessment (Y) - 20220616	47
5.18	Vertical Accuracy Assessment (Z) - 20220616	47
5.19	Horizontal Accuracy Assessment (X) - 20220715	48
5.20	Horizontal Accuracy Assessment (Y) - 20220715	49
5.21	Vertical Accuracy Assessment (Z) - 20220715	49
5.22	Detailed illustration of the DJI D-RTK 2 collector	53
5.23	Vertical Accuracy Assessment (Z) - 20230411	53
5.24	Coefficient of determination (R^2) from various DTM creation techniques - 20220601	58
5.25	Coefficient of determination (R^2) from various DTM creation techniques - 20220616	59

LIST OF TABLES

Page

3.1 Uncrewed Aerial Systems (UAS) Flights Ground Sampling Distance (GSD) 26

4.2 Ground Control Points (GCPs) Placement 35

5.3 Comparative analysis of original and resurveyed geospatial data 51

5.4 Root Mean Square Error (RMSE) X-Y-Z sumary for each GNSS method 54

5.5 Coefficient of determination (R^2) from various DTM creation techniques - 20220601 . . 57

5.6 Coefficient of determination (R^2) from various DTM creation techniques - 20220616 . . 58

CHAPTER 1: INTRODUCTION

1.1 Motivation

The motivation for this research lies at the intersection of two significant technological advances: the expanding application of geospatial technologies and the intensifying need for accurate data collection in agricultural setting. While georeferencing and Uncrewed Aircraft System (UAS) Structure-from-Motion (SfM) photogrammetry techniques have independently shown significant progress in improving data collection accuracy, there remains a lack of rigorous comparative analysis of these methods, especially within the context of plant height estimation. This study is motivated by this gap in the literature, recognizing the opportunity to provide fresh insights and propose novel recommendations for improving the accuracy and efficiency in UAS crop canopy height estimation.

Plant height is a critical factor in determining crop yield and biomass estimation, which in turn informs decision-making around resource allocation, crop health management, and growth regulator applications. This direct linkage between plant height estimation and the broader agricultural use of this trait underscores the importance of this research.

Although georeferencing techniques and UAS SfM photogrammetry have shown promise in providing reliable data for a multitude of agriculture applications, there are questions about their accuracy and effect on plant height measurements that remain unanswered. For example, how do the precision and reliability of georeferencing techniques vary when considering different Global Navigation Satellite System (GNSS) configurations? What is the influence of various Digital Terrain Model (DTM) generation methods on plant height estimation accuracy? Unveiling these complexities is fundamental to strengthening the applicability of these techniques and extending their advantages to a wider array of agricultural practices.

The rapid development of the geospatial field presents unique opportunities for advancing georeferencing techniques and UAS SfM photogrammetry. By actively seeking to contribute to this evolving discourse, this research also intends to inspire further innovation in precision agriculture and beyond.

1.2 Background

The widespread integration of geospatial technologies has been a driving force in modern precision agriculture technologies. At the heart of these advancements is the use of georeferencing techniques, UAS, and SfM photogrammetry for the measurement and estimation of plant height. Understanding the significance of these methods and their implications on plant height estimation is crucial to the progression of precision agriculture and its role in increasing crop yield, enhancing resource management, and promoting sustainability.

Georeferencing, a method used to associate geographical coordinates with digital raster image or vector database, is essential for plenty of applications, such as mapping, surveying, and remote sensing. Variations in georeferencing techniques can significantly affect the accuracy of data, thereby impacting its overall reliability and efficacy. Some commonly used georeferencing methods include GNSS-only, GNSS in conjunction with Real-Time Kinematic (RTK), GNSS in conjunction with Post-Processed Kinematic (PPK), GNSS in conjunction with Precise Point Positioning (PPP), and GNSS coupled with Real-Time Network (RTN) provided by service agencies such as the Texas Department of Transportation (TxDOT) in Texas. Despite their widespread usage, an extensive comparative analysis of these techniques, which considers factors such as precision, cost-effectiveness, and efficiency, is still lacking. Hence, it is crucial to dig into the complexities of these methods and their implications on georeferencing.

Direct and indirect georeferencing methods offer different approaches to UAS-SfM mapping and data processing. Direct georeferencing involves using onboard GNSS data coupled with Inertial Measurement Unit (IMU) data to determine the precise spatial location and orientation of the sensor at the time of image capture. On the other hand, indirect georeferencing relies on Ground Control Points (GCPs), identifiable markers on the ground that have been surveyed using precise GNSS methods. These GCPs are then identified in aerial images and are used to anchor the imagery to real-world geographic coordinates. The primary advantage of this approach is its high level of accuracy, as the GNSS surveying of the GCPs is usually done with a high level of precision. However, it is a more time-consuming process than direct georeferencing because it requires an additional surveying step and the manual identification of the GCPs in the imagery. Understanding the differences between these methods and the scenarios where each is most suitable allows for more effective and accurate georeferencing in various applications.

The technique of UAS-SfM surveys, in which a drone captures overlapping two-dimensional photos of a designated area, is involved in the creation of three-dimensional models. This approach exemplifies its remarkable potential for plant height estimation in precision agriculture. An important consideration in these surveys is the Ground Sampling Distance (GSD), which is the distance represented by one pixel's worth of data on the ground. The GSD is a crucial determinant of the spatial resolution of the resulting images and can affect the accuracy and detail of the final models. Images procured from the UAS-SfM surveys, with careful consideration of GSD, are processed using SfM algorithms to generate a 3D point cloud. This point cloud aids in the development of a Digital Surface Model (DSM) by marking the highest point in each grid cell, hence incorporating all surface objects like buildings and vegetation. Representing the bare ground surface, the creation of the DTM typically demands additional processing, often utilizing ground filtering algorithms to omit non-ground points and isolate the terrain data. Several techniques for DTM generation have been proposed, including deriving a DTM from a pre-emergence flight, interpolating ground height points, or implementing automatic classification algorithms found in software such as PIX4Dmapper. By subtracting the DTM from the DSM, a Canopy Height Model (CHM) is produced, serving as a detailed and accurate digital representation of the height of plant canopies above the ground surface. While these processes have independently shown promise in improving crop canopy height estimation, a comparative evaluation could potentially yield invaluable insights for improving the accuracy and reliability of the estimates. Precision agriculture's future growth depends on the consistent refinement of these techniques and the development of best practices tailored to the specific needs of the sector. It is within this context that this study situates itself, seeking to provide an in-depth comparative analysis of georeferencing methods and UAS SfM photogrammetry approaches, all to enhance the performance of plant height estimation.

1.3 Objectives

The overall goals of this project are:

1. To investigate and compare the accuracy and reliability of georeferencing errors derived from three distinct georeferencing methods, namely, GNSS+RTK, GNSS+RTN provided by TxDOT, and GNSS-only with and without the use of GCPs, for georeferencing of UAS-SfM 3D point cloud data.

2. To assess the correlation between manually measured plant heights and height estimations derived from UAS imagery data by comparing three different DTM generation techniques. The methods under examination include 1) utilizing a DTM obtained from a flight conducted before plant emergence, 2) creating a DTM based on interpolating ground height points, and 3) employing automatic classification algorithms available in PIX4Dmapper software.

CHAPTER 2: REVIEW OF THE LITERATURE

2.1 Precision Agriculture

Precision agriculture has carved out an essential role in contemporary farming. This role is demonstrated by its contribution to enhancing the sustainability, food safety, and security of cropping systems. This modern facet of agriculture leverages digital technologies, including smart machines, sensors similar to those found in geospatial engineering, and cloud computing to improve farming processes Carolan (2017). This point is exemplified by a 2018 research project funded by Università Politecnica delle Marche titled ”PFRLab: Setting of a precision farming robotic laboratory for cropping system sustainability and food safety and security.” This project underlines the potential of precision agriculture to revolutionize crop management Barbedo (2016). As part of the project, the interdepartmental Research and Services Center ”Smart Farming” was established to strengthen multidisciplinary collaborations in agriculture Regan (2019).

In recent years, the use of UAS in agriculture has gained significant momentum due to their versatility and ability to provide high-resolution data in a cost-effective and efficient manner Sankaran et al. (2015). The integration of UAS technology with advanced georeferencing techniques and remote sensing approaches has opened up new avenues for improving the accuracy and precision of plant height estimation in precision agriculture. Precision agriculture has emerged as a cornerstone of contemporary farming, fostering sustainability and bolstering food safety and security in cropping systems. The utilization of digital technologies combined with the adoption of conservation agriculture and precision farming techniques is propelling a shift from traditional agricultural practices to more sustainable and efficient methods Fountas et al. (2015).

In precision agriculture, the use of UAS for remote sensing has gained significant attention. A study conducted by Stanton et al. (2017) demonstrated the effectiveness of using a small, fixed-wing UAS to monitor a field experiment designed to evaluate the impact of aphid infestations on sorghum crops. The UAS, equipped with a consumer-grade near-infrared camera, was used to create normalized difference vegetation index (NDVI) maps and three-dimensional point clouds of the experimental plots. The researchers found that NDVI and plant height metrics averaged on a per-plot basis, were capable of identifying aphid-induced plant stress. Furthermore, the study revealed that the NDVI calculated from UAS imagery, when compared with measurements from sensors on a manned aircraft and a tractor, showed a dependence on the growth stage. Interestingly, the researchers noted negative correlations between aphid density and NDVI, particularly toward the end of the growing season in the most damaged crops.

2.1.1 Advancements in UAS technology for agricultural applications

One of the major advancements in UAS technology is the integration of multispectral and hyperspectral imaging sensors, which enable the simultaneous capture of information across multiple spectral bands. These sensors facilitate the extraction of biophysical and biochemical parameters of crops, such as Leaf Area Index (LAI), water content, and nutrient content, leading to more accurate and timely monitoring of crop health and growth Tattaris et al. (2016). Additionally, the development of lightweight and compact sensors has made it easier to mount them on UAS platforms, further expanding their utility in agricultural applications Sankaran et al. (2015).

Another key advancement is the improvement in UAS flight planning and control systems. Modern UAS platforms are equipped with autonomous flight capabilities, enabling them to cover large areas and follow pre-defined flight paths with minimal human intervention. This not only reduces the time and labor required for aerial surveys but also ensures that data is collected consistently across different flights and periods.

The fusion of UAS-derived data with other geospatial datasets, such as satellite imagery and LiDAR, has also gained traction in recent years. This integration allows for the development of more comprehensive and accurate geospatial models that can be used to estimate plant height and other crop parameters Xie & Yang (2020).

Machine learning and artificial intelligence (AI) techniques have further contributed to the advancement of UAS technology for agricultural applications. By applying these techniques to the processing and analysis of UAS-derived data, researchers have been able to develop more accurate and efficient models for tree height estimation Torres-Sánchez et al. (2018). Deep learning algorithms, in particular, have demonstrated promising results in extracting complex features from multispectral and hyperspectral imagery, leading to improved estimation of crop parameters Kefauver et al. (2017).

2.2 Remote Sensing for Precision Agriculture

UAS SfM photogrammetry has played a crucial role in precision agriculture which is an essential agronomic and phenotypic trait X. Wang et al. (2019a). Accurate crop height measurements facilitate the estimation of biomass Bendig et al. (2013a) ; B. Li et al. (2020), yield Feng et al. (2020) ; Geipel et al. (2014), and plant nitrogen usage Eitel et al. (2014) ; Barrero Farfan et al. (2013), as well as the quantification of lodged areas Berry & Spink (2012) ; S. C. Chapman et al. (2014). Traditional methods of measuring crop height, such as using a ruler, are labor-intensive, inefficient, and susceptible to human error Khan et al. (2018) ; Watanabe et al. (2017).

Alternative remote sensing approaches for crop height estimation include ultrasonic sensors and Light Detection and Ranging (LiDAR). Ultrasonic sensors have been employed for crop height measurement in agriculture applications for many years Andrade-Sanchez et al. (2013) ; Chang et al. (2017) ; Barker et al. (2016). However, these sensors have limitations, such as a decrease in measurement accuracy due to the wide-angle divergence of ultrasonic waves and sensitivity to temperature variations Llorens et al. (2011) ; Sun et al. (2017). LiDAR finds gaps and penetrates in that manner through vegetation, allowing for vertical classification of crop and soil surfaces Andrews et al. (2013) ; Grenzdörffer (2014). Yet, its use in estimating crop height for low-stature plants is limited due to the high cost and large volume of data obtained, which can be difficult to process Jayathunga et al. (2018) ; Maimaitijiang et al. (2019); Yuan et al. (2018).

2.2.1 UAS Approaches

UASs combined with high-resolution digital cameras have emerged as a promising platform for obtaining crop height information due to their low cost, high flexibility, and high spatial resolution A. et al. (2019) ; W. Li et al. (2016); Malambo et al. (2018). SfM algorithms enable the production of geometrically precise 3D point clouds from a set of overlapping images obtained by RGB sensors H. et al. (2016) ; P. Hu et al. (2018) ; Hammerle & Hofle (2016); Malambo et al. (2018). The quality of point clouds generated using SfM algorithms is comparable to those produced by LiDAR, which is crucial for the precise study of crop structure A. et al. (2019) ; W. Li et al. (2016).

However, obtaining accurate crop height estimates typically requires at least two flight missions, a non-vegetated digital terrain model (DTM) shortly after sowing or harvesting, and a digital surface model (DSM) during the season when crop height needs to be measured. GCPs are also important for georeferencing among multi-temporal images Bendig et al. (2015a). In many studies, complete spatial auxiliary (SA) information was not used for crop height estimation due to the experimental cost or feasibility of data collection B. Li et al. (2020) ; A. J. Mathews & Jensen (2013) ; Tao et al. (2020).

2.3 Structure-from-Motion Phtogrammetry

Drawing from Starek & Wilkinson (2022), the following text provides a detailed overview of the use of SfM in UAS mapping applications, outlining the processing workflow and data collection methods. SfM, a type of photogrammetry employed in processing imagery from small UAS, relies heavily on acquiring sufficient overlap. This overlap can be broken down into two types: frontal overlap with respect to the flight direction (or endlap), and side overlap between flight lines (or sidelap). The importance of overlap becomes evident when considering the nature of small UAS photogrammetric surveys, which are typically processed using a technique known as Structure-from-Motion/Multi-View Stereo (SfM/MVS) photogrammetry.

Traditional photogrammetry techniques necessitate the use of precisely calibrated metric cameras, which are typically expensive and thus not ideal for widespread UAS mapping applications. To circumvent this issue, SfM uses information from multiple overlapping images to extract 3D object data, eliminating the need for precise camera calibration. SfM accomplishes this by deriving three-dimensional structures from two-dimensional image sequences that are obtained through the movement of the camera, providing different perspective views of the scene. In this scenario, the UAS functions as the moving platform, facilitating the implementation of SfM with an onboard camera by acquiring images with sufficient overlap.

The SfM processing workflow consists of several stages, starting with Keypoint Extraction and Matching. In this initial stage, image sequences are input into the software, and a keypoint detection algorithm, such as the scale-invariant feature transform (SIFT), is used to automatically extract features and find keypoint correspondences between overlapping images. Keypoints are points of interest on the UAS images that can be easily recognized by the SfM software's automated keypoint extraction and correspondence algorithms.

The next stage, Bundle Adjustment and Sparse Point Cloud Creation, involves an iterative least squares bundle adjustment to minimize the errors in the keypoint correspondences. This is achieved by automatically solving for camera interior orientation parameters and performing aerial triangulation to resolve the relative orientation parameters of the camera at the time of image acquisition. The matching points are then verified, and their 3D coordinates are simultaneously calculated to generate a sparse point cloud.

This point cloud is then georeferenced using either GCPs or camera geolocations provided by an onboard GNSS receiver. This step allows the exterior orientation parameters of the camera and the coordinates of the sparse point cloud to be constrained to a geodetic coordinate system. The solution can rely solely on the direct georeferencing provided by the onboard GNSS receiver, or GCPs can be applied to optimize the solution.

Finally, the last stage, 3D Point Cloud Densification, uses the interior and exterior orientation for each image as input into an MVS algorithm. This algorithm attempts to densify the point cloud by projecting every pixel at the full image scale or projecting pixels at a reduced image scale. The result of the UAS-SfM image processing workflow is a densified set of X-Y-Z coordinates of the imaged scene, referred to as a point cloud. This point cloud, typically colorized by the RGB pixel values of the digital camera, can have a high point density due to the high camera resolutions and typical low altitudes at which data are collected. The 3D point cloud can then be used to generate a digital surface model of the terrain, which can subsequently be used to orthorectify the images and produce an orthomosaic image or a 3D textured mesh.

A typical SfM image processing workflow is as follows 2.1 from A. Mathews (2021).

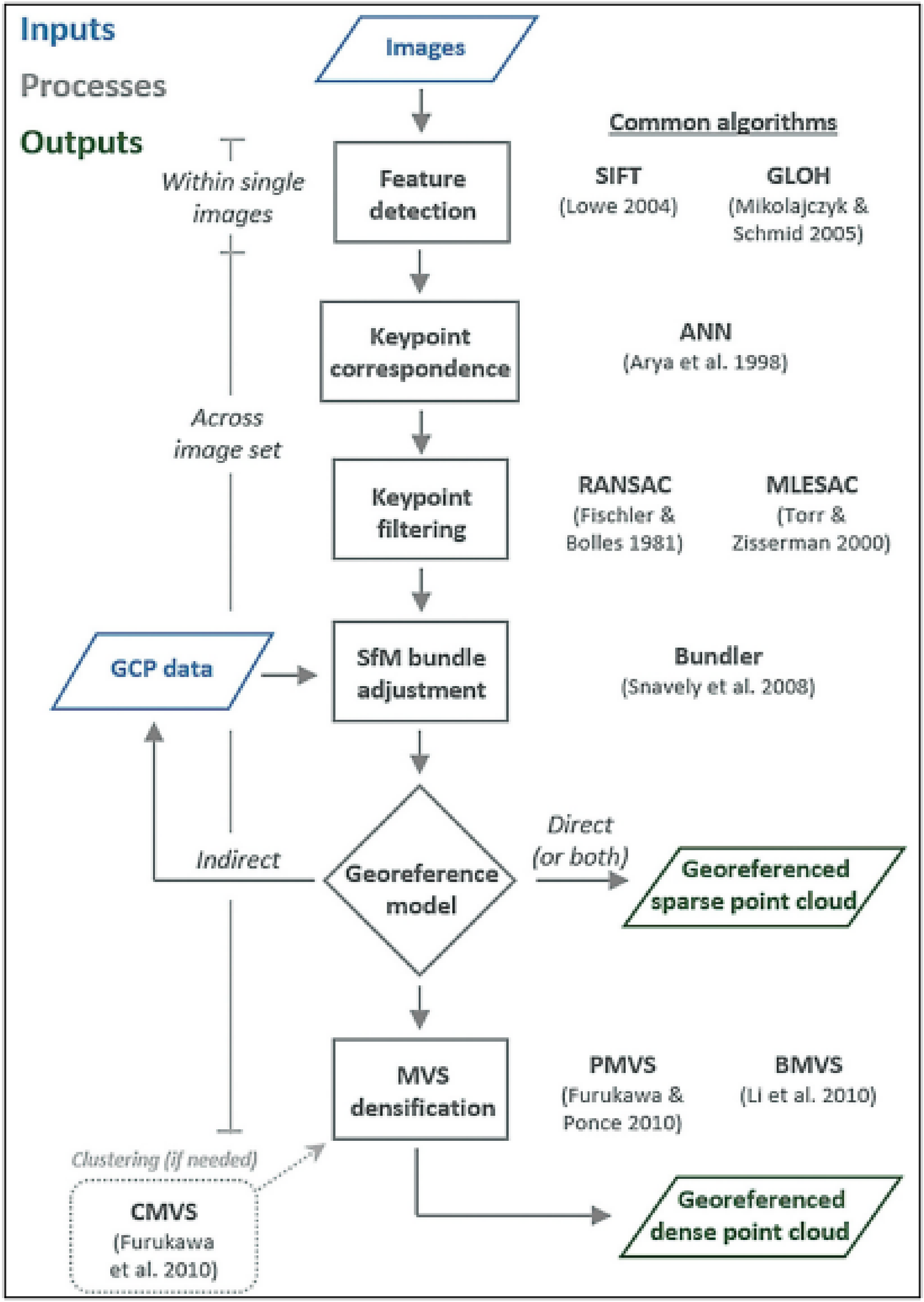

Figure 2.1
SfM process flow, highlighting the primary stages and frequently employed algorithms. The main inputs into the SfM image processing workflow, namely aerial photos captured by drones and GCPs collected in the field, are utilized to generate georeferenced sparse and dense point clouds.

2.3.1 Georeferencing methods for UAS-SfM

Georeferencing is a complex, labor-intensive process that requires skilled interpretation of location information A. Chapman & Wieczorek (2020). Automating this process has been challenging due to factors such as awareness, collection management systems, staff workload, tool friendliness, and geographic features Marcer et al. (2021). To overcome these challenges, it is necessary to enhance resource availability, provide centralized support, develop better-automated tools, improve databases, and share user stories that promote better georeferencing practices Marcer et al. (2021). By refining existing procedures and working collectively, the global collections and research communities can harness the immense value of natural history collections, enabling new and broader applications of the global collections resource for research and public interpretation Marcer et al. (2021).

Topographic data with high resolution generated by SfM photogrammetry is initially produced within an arbitrary reference frame. This means that these data points do not have a standardized spatial context in the first stages of processing. Dinkov (2023) The process of georeferencing, as described by Harwin & Lucieer (2012), is the transformation of this initial arbitrary data into a predefined coordinate reference system. This transformation process is pivotal in providing the data with a standardized spatial context, which can be understood and utilized in further analyses.

Georeferencing can be carried out in two ways: direct and indirect georeferencing. Direct georeferencing employs known external parameters of the photographs. This method utilizes information about the camera's position and orientation at the time each photograph was taken. This information, often collected from an onboard GNSS receiver and an inertial measurement unit (IMU), enables the direct linking of image data to real-world geographic coordinates.

On the other hand, indirect georeferencing, as discussed by Sanz-Ablanedo et al. (2018), involves assigning appropriate coordinates to specific points GCPs that can be recognized in the images. GCPs are physical markers or natural features present in the landscape that have been surveyed with high-accuracy positioning equipment. These points are used to anchor the arbitrary SfM data to real-world coordinates. This method allows for the connection of visual features in the photographic data to actual geographic locations, providing the necessary spatial context for further interpretation and analysis.

2.3.1.1 GNSS+RTK

In the "Unoccupied Aerial Vehicle Derived 3D Model Evaluation Based on Icesat-2 for Ice Surface Micro-Topography Analysis in East Antarctica" article, the DJI D-RTK GNSS technology was implemented for UAS-derived ice sheet micro-topography modeling without GCPs in a study focused on East Antarctica He et al. (2021). This technology has shown great potential for enhancing geospatial accuracy and precision in digital agriculture as well.

The DJI UAS technology, including DJI Phantom 4 RTK and D-RTK GNSS mobile station, was employed in this study to obtain a high-precision UAS photography position without the need for GCPs He et al. (2021). This is particularly useful in extreme climate conditions, such as Antarctica, where establishing a ground control network can be challenging. The GNSS RTK technology and precise point positioning (PPP) technology were used to determine the position of the base station, while the UAS flight used differential positioning with a dual-frequency receiver to eliminate ionospheric delay He et al. (2021).

The study found that the vertical accuracy of UAS-SfM generated 3D models without GCPs decreases significantly with distance to the D-RTK GNSS mobile station, especially in areas with great gradient variation He et al. (2021). The results indicate that the DJI UAS technology can achieve acceptable results without ground measurement support in some extreme polar scenarios. In future applications, distance to the D-RTK GNSS mobile station and terrain should be considered as the main error sources for UAS model reconstruction He et al. (2021).

The study concluded that the DJI UAS technology has the potential to be applied for ice surface micro-topography detection if the distance to the D-RTK GNSS mobile station and terrain are considered He et al. (2021). The use of virtual GCPs and suitable mathematical correction models could improve the limitations found in this study, expanding UAS applications in polar regions.

2.3.1.2 GNSS+RTN

In recent years, advances in GNSS positioning technology have led to the development of RTN to enhance geospatial accuracy and precision. RTN systems, such as the one provided by TxDOT, offer several advantages over traditional RTK solutions Ouml et al. (2010). For instance, RTN systems do not require users to set up a physical base station, as they tap into an existing network of established and error-corrected stations within the system's coverage area Dao et al. (2004).

RTN systems have demonstrated improved accuracy over RTK systems, with documented accuracy better than 4 cm vertically and 1-6 cm horizontally G. R. Hu et al. (2002). The increased accuracy and precision provided by RTN systems have significant implications for various applications, including precision agriculture, which demands highly accurate geospatial data for plant height estimation and other aspects of crop management Ali (2012).

One study comparing the precision performance of RTK and RTN systems in Los Angeles County, California, found that the vertical precision for RTN measurements was 2-4 times lower than that of RTK measurements Benjamin et al. (2020). The findings suggest that RTN systems could potentially deliver superior accuracy and reliability in positioning data, particularly within complex settings where standard RTK systems may grapple with challenges such as atmospheric gradient. However, it should be noted that RTN systems does not resolve issues related to multipath Kaloop et al. (2020) ; Rovira-Garcia et al. (2020).

2.3.1.3 GNSS+PPK

The use of PPK solutions in a UAS has been evaluated for geospatial accuracy in forested areas. PPK is one of the two primary modifications of kinematic GNSS measurements for UAS applications, where corrections from a virtual reference station (VRS) are applied post-flight. The objective of the study conducted by Tomaštík et al. (2019) was to compare the accuracy of photogrammetric products obtained from the UAS PPK solution with the traditional approach of using GCPs for georeferencing. The study also examined the influence of vegetation season and flight patterns on the accuracies. The results showed that the PPK solution provided lower horizontal and vertical errors compared to the GCP approaches. Horizontal errors for PPK did not exceed 10 centimeters, while vertical errors remained under 20 centimeters. In contrast, the GCP solutions exhibited higher errors, with the highest horizontal error reaching 28.2 centimeters and the highest vertical error reaching 58.1 centimeters. The study concluded that the PPK method can provide highly accurate spatial data comparable to the GCP approaches, making it a promising solution for mapping inaccessible and hazardous forest areas.

2.3.1.4 GNSS+PPP

PPP is a widely studied method for determining the coordinates in GNSS surveys without the need for a nearby reference station. It is a global positioning method that relies on measurements from multiple satellite constellations, such as GPS, GLONASS, Galileo, and BeiDou. The comparison of PPP with other survey methods, such as RTN and static modes, has been a topic of interest in scientific and technical applications. However, evaluating the accuracy of the static mode solution, which is often used as the reference, can be challenging due to various parameters that need to be considered. Dardanelli et al. (2021) aimed to compare the performance of PPP, NRTK, and static methods by analyzing the solutions obtained from benchmark points. The tests were conducted by comparing the solutions in pairs and assessing their congruence. The RTN and static solutions were based on a local GNSS CORS network analysis, while the PPP solution was obtained using two different software packages. Statistical analysis was performed to determine the distribution frequencies of the coordinate residuals and assess their conformity to a normal distribution. The results showed that the Static vs. RTN pair showed the lowest range of variability and the lowest standard deviation.

2.3.1.5 Standalone GNSS

Standalone GNSS receivers have become popular due to their reconfigurable and flexible design, low price, and the possibilities of new specifications and algorithms that can be exploited (Paziewski (2020)). In recent years, software-defined radio (SDR) technology and Free-and-Open-Source Software (FOSS) have changed the landscape, with software-defined receivers (SDRs) providing extreme customization and allowing users to access, visualize, and modify signal acquisition, tracking, and processing strategies. Many software solutions in GNSS positioning now follow the

SDR approach, such as GSNRx, ipexSR, N-Gene, and combined GPS and GLONASS software receivers Petovello et al. (2008); Marco et al. (2001); Maurizio et al. (2009); S. & Mark (2008); Lee & Park (2002).

One example of an open-source software solution for GNSS signal processing is GNSS-SDR, which is capable of acquiring, processing, and computing navigation solutions for different constellations such as GPS, GLONASS, and Galileo Carles et al. (2011). In the work by Matteo et al. (2019) and Matteo et al. (2020), the quality of the pseudo ranges generated by an ultra-low-cost front-end driven by a software-defined receiver was assessed through code-minus-carrier (CMC) analysis. This study compared the performance of the SDR against a low-cost commercial-of-the-shelf (COTS) receiver, the UBX z-f9p.

The results showed that the SDR was not able to acquire all the satellites tracked by the UBX, and those satellites were characterized by a low signal gain. The CMC analysis confirmed the presence of more noise in the observables generated by the SDR. Furthermore, the positioning performance obtained by the SDR was worse than that of the UBX in all scenarios, with the mean and standard deviation of the UBX horizontal error being about half of those of the SDR Matteo et al. (2020).

These findings suggest that the limitations of the ultra-low-cost front-end used in the Rafael micro-SDR driven by GNSS-SDR configuration are the main cause of the noisy measurements and poor positioning performance. Future work could involve a denoising step of the observables to improve the positioning algorithm, testing various RF front-ends to assess the influence of hardware on overall performance, and conducting an in-depth pseudo-range errors analysis Matteo et al. (2020).

2.3.1.6 Comparison of accuracy and efficiency

Standalone GNSS is a widely used geospatial positioning technique that employs satellites to provide location and time information Alfred et al. (2015). In agricultural applications, the accuracy of GNSS-only is often limited to a few meters, making it unsuitable for high-precision tasks such as plant height estimation.

In comparison, GNSS+RTK and GNSS+RTN techniques offer higher accuracy. RTN utilizes a network of fixed reference stations that continuously transmit corrections to improve the positioning accuracy of mobile receivers Mora et al. (2022). RTK, on the other hand, employs a base station and a rover to compute real-time differential corrections, resulting in centimeter-level accuracy K. Wang & El-Mowafy (2021).

While the accuracy of RTN and RTK is superior to GNSS-only, the cost of implementing these techniques is often higher. Standalone GNSS receivers are more affordable, making them an attractive option for small-scale farmers. However, the lower accuracy may lead to inefficiencies in agricultural operations, resulting in increased costs over time Javier et al. (2020).

In contrast, RTN and RTK systems require more sophisticated equipment and infrastructure, increasing the initial investment Mora et al. (2022); K. Wang & El-Mowafy (2021). Despite the higher costs, the improved accuracy offered by these techniques can lead to substantial savings in the long run by optimizing agricultural practices and reducing resource waste Javier et al. (2020).

In terms of efficiency, GNSS+RTK and GNSS+RTN provide real-time corrections, allowing for immediate and accurate positioning Mora et al. (2022) ; K. Wang & El-Mowafy (2021). This is particularly advantageous in precision agriculture, where timely decision-making is crucial for optimal crop management.

Standalone GNSS, while less accurate, still offers some benefits in terms of efficiency. The simplicity of the technology and its widespread availability make it easy to deploy and use in various agricultural settings Alfred et al. (2015). However, the lower accuracy may result in inefficient agricultural practices, which could negate some of the benefits of its ease of use.

2.4 UAS SfM & LiDAR for Crop Height Monitoring

2.4.1 UAS-SfM for Crop Height Monitoring

Estimating plant height is a crucial aspect of precision agriculture, as it provides valuable information on crop growth and productivity Bendig et al. (2015b). UAS have emerged as a promising tool for plant height estimation due to their ability to acquire high-resolution imagery and flexibility in data acquisition Zhang et al. (2022).

UAS-based plant height estimation generally involves two main steps: (1) deriving a DSM representing the top of the vegetation and (2) subtracting a DTM or DEM representing the ground surface to obtain the plant height Duan et al. (2017). Various methods have been proposed for generating DSMs and DTMs from UAS imagery, such as SfM photogrammetry, LiDAR, and stereo vision techniques Zhang et al. (2022).

SfM photogrammetry is a widely used technique for generating high-resolution DSMs and DTMs from UAS-derived imagery. It involves the extraction of 3D information from a sequence of 2D images captured at different viewpoints Westoby et al. (2012). SfM has been employed in numerous studies for plant height estimation, demonstrating its effectiveness and accuracy in different agricultural contexts Zhang et al. (2022).

2.4.2 UAS-LiDAR for Crop Height Monitoring

LiDAR sensors can also be mounted on UAS platforms for direct 3D point cloud generation. UAS-based LiDAR has shown great potential for plant height estimation due to its ability to find gaps and penetrates in that manner through vegetation, providing accurate ground surface information Wallace et al. (2012). Recent advancements in lightweight and compact LiDAR sensors have made it increasingly feasible to integrate them with UAS platforms for agricultural applications Zhang et al. (2022). LiDAR technology presents a promising avenue for crop height monitoring. A study by Hütt et al. (2022) demonstrated the effectiveness of LiDAR scanners mounted on UAVs in overcoming the shortcomings of traditional remote sensing techniques, such as poor area efficiency, long post-processing requirements, and the inability to simultaneously capture ground and canopy data. Their research utilized a RIEGL Mini-VUX-1 LiDAR scanner on a DJI Matrice 600 PRO UAV to acquire a point cloud from a winter wheat field trial. Through the analysis of the UAS-derived LiDAR point cloud and the application of LiDAR metrics traditionally used in forest monitoring, it was found that the 95th percentile of the height of normalized LiDAR points correlated strongly with manually measured crop heights and crop heights derived from a UAS with optical imaging. The study further demonstrated the potential of UAS LiDAR metrics in estimating crop traits like dry biomass (DBM) and nitrogen uptake, making it a promising tool for crop height monitoring and trait estimation in precision agriculture.

UAS-based plant height estimation has demonstrated great potential in precision agriculture, with various techniques such as SfM photogrammetry, and LiDAR being employed to generate accurate DSMs and DTMs.

2.5 DTM Generation Techniques

2.5.1 DTM obtained from a pre-plant emergence flight

DTMs obtained from pre-plant emergence flights play a significant role in crop height estimation Bendig et al. (2013b). This method requires at least two flight missions, one shortly after sowing or harvesting to capture the non-vegetated terrain and another during the season when crop height needs to be measured. According to Bendig et al. (2015c), the resulting DTM from the pre-plant emergence flight represents the ground surface, which aids in the subsequent estimation of plant heights. This approach is crucial for ensuring the accuracy of crop height estimation when the field terrain is uneven. However, the technique is reliant on the availability of UAS platforms and the feasibility of carrying out multiple flights Feng et al. (2019).

2.5.2 DTM based on interpolating ground height points

Another commonly used approach to generate DTMs involves interpolating ground height points. Feng et al. (2019) applied this technique by splitting the study field into small plots to obtain bare ground elevation. They then conducted linear interpolation of the soil surface elevation between adjacent plots to calculate the elevation of the bare ground that was not visible. This method provides a solution to situations where it is difficult to obtain the DTM accurately from the DSM when the crop canopy is closed. However, this method still requires a considerable amount of labor for ground point data collection and interpolation Yue et al. (2017).

2.5.3 DTM created using automatic classification algorithms in PIX4Dmapper

Recently, automatic classification algorithms, like those employed in PIX4Dmapper software, have been used to create DTMs. Agisoft Photoscan software, similar to PIX4Dmapper, was used by Liang et al. (2019) and Yilmaz et al. (2018) to classify dense point clouds into ground point clouds and generate the DTM by interpolation based on the classified ground point clouds. This approach is efficient and reduces the need for manual extraction of ground points from the DSM. However, it requires sophisticated software and an understanding of the classification algorithms.

2.5.4 Comparison of accuracy and reliability

Each of these methods has strengths and weaknesses, and the choice of method depends on various factors including the availability of resources, the nature of the terrain, and the specific requirements of the crop height estimation task. Regardless of the method used, it is crucial to take into account the potential sources of error and the need for accuracy in plant height estimation in precision agriculture X. Wang et al. (2019b).

CHAPTER 3: MATERIALS & METHODS

3.1 Study Location

The study was conducted at the Texas A&M AgriLife Research and Extension Center, situated in Corpus Christi, Texas, USA, with geographical coordinates of 27°46’35”N latitude and 97°33’38”W longitude as shown in figure 3.2. The research focused on corn crops cultivated during the 2022 agricultural growing season, leveraging the center’s resources and expertise in crop management and agronomic practices. The selection of this location allowed for the comprehensive evaluation of georeferencing techniques and UAS-based plant height estimation methods under real-world conditions, ensuring that the results and insights generated from this study are both relevant and applicable to the broader agricultural community. As shown in figure 3.2, the study area contained a corn field with a unique characteristic - it contained three distinct planting dates, each providing a different stage of crop growth. This entire area was considered in the georeferencing study. However, for the plant height estimation study, attention was focused solely on the third planting date. This targeted area, which offered a snapshot of the least mature growth stage, spanned an area of 40 x 40 meters. Over this area, a total of 36 sections with at least 6 plants were selected to measure plant height.

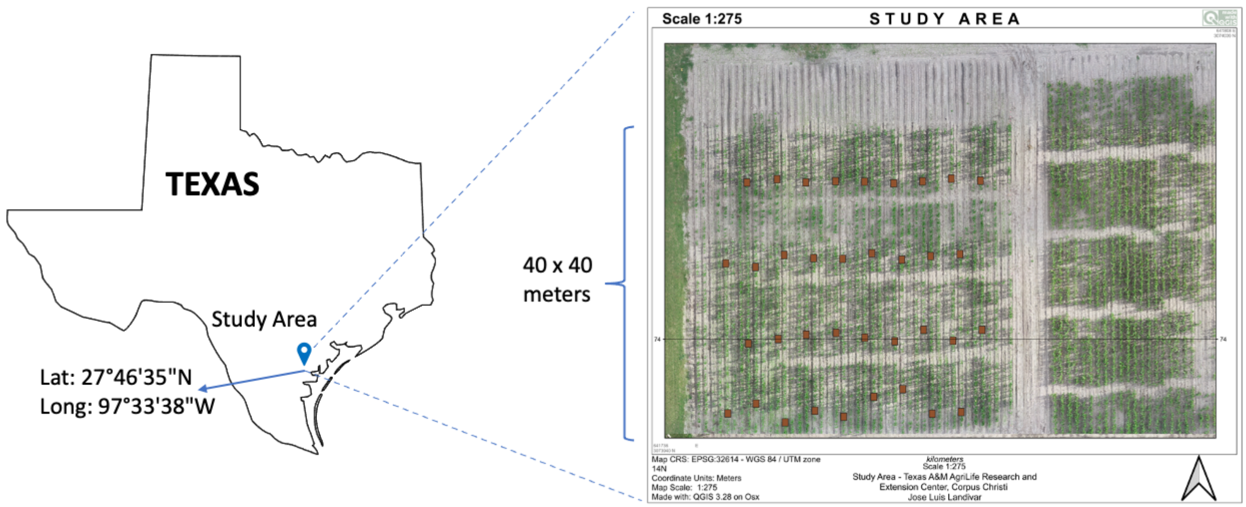

Figure 3.2
Texas A&M AgriLife Research and Extension Center, situated in Corpus Christi, Texas and corn Field with 36 plot boundaries from which plant height was measured and estimated.

3.2 Equipment & Tools

3.2.1 UAS Platform & GNSS receiver

In this study, a range of state-of-the-art geospatial hardware was employed to accurately and efficiently collect the data necessary for the research of georeferencing systems comparison and UAS-based plant height estimation. The primary equipment utilized in the research included the Emlid Reach RS2 GNSS receiver, the DJI Phantom 4 RTK drone, and the DJI D-RTK 2 Mobile Station (see figure 3.3).

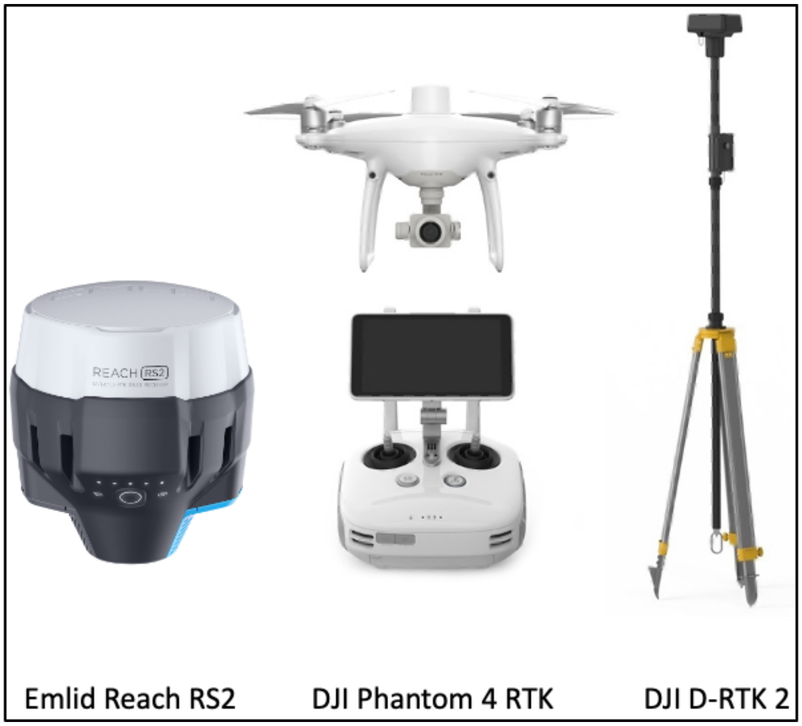

Figure 3.3
Hardware used for data collection in this study, including Emlid Reach RS2, DJI Phantom 4 RTK, and DJI D-RTK 2 Mobile Station.

The Emlid Reach RS2 is a compact and rugged GNSS receiver. This receiver offers multi-band GNSS support, enabling it to track GPS, GLONASS, BeiDou, Galileo, QZSS, and SBAS satellite systems. Its L1, L2, and L5 frequency bands provide improved positioning accuracy, faster convergence times, and enhanced robustness against interference and multipath effects. In this study, a pair of Emlid Reach RS2 devices were employed for the precise acquisition of Ground Control Points (GCPs) location data, aiming to assess the comparative performance of various georeferencing techniques during aerial data capture. The devices were utilized in distinct roles: one Emlid Reach RS2 functioned as a rover station for pinpointing GCPs, while the second operated as the base station. Notably, even though Emlid Reach RS2 possesses the capacity to receive RTN corrections, this functionality was not employed in this study.

The DJI Phantom 4 RTK, released in October 2018, is an advanced aerial mapping platform that combines the high-resolution imaging capabilities of the DJI Phantom 4 series with RTK technology for centimeter-level positioning accuracy. The drone's integrated RTK module allows for direct georeferencing of the captured imagery, significantly reducing the need for GCPs and streamlining the post-processing workflow.

The DJI Phantom 4 RTK has a three-axis stabilized camera with a high-resolution 1-inch (25 mm) 20 MP CMOS sensor FC6310, ensuring the captured aerial imagery exhibits exceptional detail and clarity. The sensor's large size allows for enhanced low-light performance and improved dynamic range, resulting in superior image quality across various lighting conditions. The camera features a mechanical shutter, which minimizes rolling shutter distortion, a common issue in aerial imagery captured at high speeds or low altitudes. The Phantom 4 RTK camera has a 24mm (35mm equivalent) lens with an 84° field of view, providing broad coverage while maintaining a sharp, distortion-free image. With a maximum resolution of 5472x3648 pixels, the drone can capture high-resolution aerial imagery, allowing for the generation of accurate and detailed orthomosaics, digital surface models, and digital terrain models, which are crucial components of this study's georeferencing systems comparison and plant height estimation analysis.

The DJI D-RTK 2 Mobile Station is a high-precision GNSS receiver specifically designed to work in conjunction with DJI's RTK-enabled drones, such as the Phantom 4 RTK. This mobile station provides real-time differential corrections to the drone's RTK module, ensuring centimeter-level accuracy in the geolocation data of the captured imagery. In the context of this study, the DJI D-RTK 2 Mobile Station was deployed under operation mode 1 to facilitate the high-precision georeferencing of aerial images acquired by the Phantom 4 RTK. This enabled the precise evaluation and comparison of the various georeferencing techniques under investigation. Notably, when functioning as a base station, the DJI D-RTK 2 Mobile Station could operate utilizing pre-measured coordinates and altitude data for setup. These coordinates were gathered beforehand with alternative survey equipment. Consequently, there was no requirement for the station to remain stationary for a minimum of two hours to establish its precise coordinates and altitude.

TxDOT RTN is a type of high-precision, networked GNSS positioning infrastructure provided and maintained by TxDOT. It includes a series of permanent GNSS stations, also known as regional reference points, spread across Texas that continuously collect and transmit GNSS data. These stations allow users within that area to receive corrected positioning data in real-time, significantly increasing the accuracy of their GNSS receivers. Figure 3.4 provides an overview of the 194 TxDOT Regional Reference Points (RRPs) and RTN across the state. For this project, the Corpus Christi station, with station code txcc, was utilized to provide RTN signals in real-time to the Phantom 4 RTK platform. It is located at latitude 27.7407931, longitude -97.44166959, and ellipsoid height of -9.086 (coordinate type: NGS CORS)

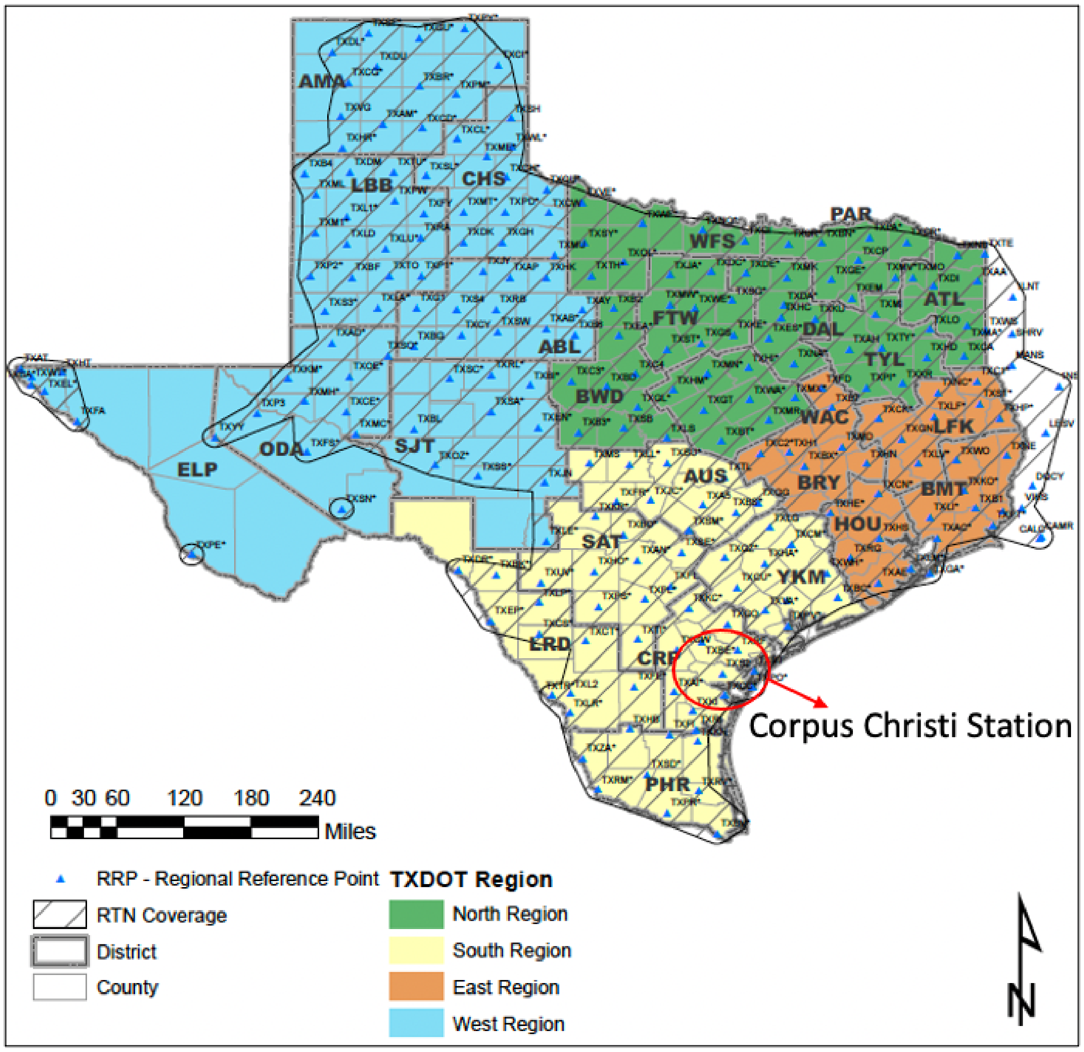

Figure 3.4
Geographical location of TxDOT RTN 194 high-accuracy base stations across the state of Texas as of September 2022.

3.2.2 PIX4Dmapper & QGIS

In this study, two prominent geospatial software tools were employed to process and analyze the collected data, ensuring that the findings were generated using the latest industry-standard methodologies. The software packages used in this research were PIX4Dmapper (Version 4.7.5) and QGIS (Version 3.22.14-Bialowieza). These tools were selected for their proven capabilities in handling a wide range of geospatial data types, as well as their compatibility with the hardware utilized in the study. Each software played a critical role in the data processing, extraction, and analysis stages of the research, allowing for a comprehensive evaluation of georeferencing systems comparison and plant height estimation methods.

PIX4Dmapper (Version 4.7.5) is a powerful SfM/multi-view stereo photogrammetry software suite designed for processing aerial and terrestrial imagery, converting the collected data into highly accurate georeferenced 2D and 3D models. In this study, PIX4Dmapper was used to process the aerial imagery captured by the DJI Phantom 4 RTK drone, generating high-resolution orthomosaics, DSMs, and DTMs for further analysis. The software's robust algorithms facilitated the automatic classification of ground points, which enabled the comparison of the various DTM generation techniques under investigation. Additionally, PIX4Dmapper's quality assessment tools were instrumental in assessing the accuracy and precision of the georeferenced imagery produced using the different georeferencing methods, as well as calculating georeferencing systems comparison by leveraging the GCPs established by the Emlid Reach RS2 GNSS receiver.

QGIS (Version 3.22.14-Bialowieza) is a widely recognized, open-source Geographic Information System (GIS) software that provides extensive data handling and analysis capabilities. In this research, QGIS was employed to analyze and extract the geospatial data generated by PIX4Dmapper, including the orthomosaics, DSMs, DTMs, and canopy height models (CHMs). Plant height was extracted from the CHMs, which were derived by subtracting the DTMs from the DSMs, effectively isolating the height of the vegetation above the ground. The Zonal Statistics tool in QGIS enabled the extraction of values for specific areas, allowing for a detailed assessment of plant height within the experimental boundaries. By leveraging the capabilities of QGIS, the study effectively extracted and analyzed plant height data from the processed imagery, enabling the comparison of the different methods to obtain DTMs and the evaluation of their performance in real-world agricultural applications.

3.3 Data Collection

3.3.1 UAS Flights

In this study, a series of UAS flights using an RGB camera on a DJI Phantom 4 RTK platform were meticulously planned and executed to capture high-resolution aerial imagery of the experimental site for subsequent processing and analysis. Five flights were conducted - 03/26/2022, 06/01/2022, 06/16/2022, 07/15/2022, and 04/11/2023 - to ensure that the results could be validated through repetition, thus enhancing the reliability of the research findings. These UAS flights were designed to provide the necessary data for comparing various georeferencing and plant height estimation methods while considering factors such as altitude, flight speed, overlap, and planning method. GSD for each flight is shown in table 3.1.

Table 3.1
GSD for each flight at that 25 meters AGL.

UAS Flight Date	**GSD [cm]**
03/26/2022	0.77
06/01/2022	0.77
06/16/2022	0.75
07/15/2022	0.74
04/11/2023	0.74

The UAS flights were performed at an altitude of 25 meters above ground level (AGL), which is the lowest altitude permissible for the DJI Phantom 4 RTK. Flying at this low altitude allowed us to obtain the highest possible resolution for the captured imagery, directly contributing to more accurate results in plant height estimation. The flight speed was set at 2 meters per second, a deliberate choice to strike a balance between data collection efficiency - the ability to gather the maximum amount of relevant and accurate data with minimal time and energy - and the level of detail required for accurate georeferencing and plant height estimation. To achieve optimal coverage and image quality, the front and side overlap were set to 80%, ensuring a sufficient level of redundancy in the captured images to facilitate accurate and reliable photogrammetric processing. When setting up the UAS mission on the remote controller, the planning method selected was ”Photogrammetry 2D”, which is well-suited for this type of agricultural study, as it allows for the generation of detailed orthomosaics and elevation models. These carefully chosen parameters were specifically designed to maximize the quality of the UAS-SfM data collected and the accuracy of the subsequent analyses, ultimately enhancing the reliability and robustness of the research findings.

Prior to the three core experimental flights (06/01/2022, 06/16/2022, and 07/15/2022), a preliminary flight took place on 03/26/2022 to obtain a DTM before plant emergence. For the georeferencing objective of this study, the DJI D-RTK 2 Mobile Station was used for georeferencing during all flights, providing real-time differential corrections to the DJI Phantom 4 RTK drone’s onboard RTK module and ensuring centimeter-level accuracy in the geolocation data of the captured imagery.

Building on the findings from the initial four flights, an additional UAS flight was carried out on 04/11/2023 to specifically assess the accuracy of aerial imagery when using the DJI D-RTK 2 Mobile Station after changing the input parameters of its known location. The goal of this flight was to evaluate the performance and reliability of GNSS+RTK in providing accurate georeferencing information. By examining the impact of modified input parameters on georeferencing accuracy, the research aimed to improve the previously obtained results and understanding of how such changes affect the overall quality and precision of geospatial data generated, ultimately contributing to the development of best practices for using GNSS+RTK in geospatial projects.

3.3.2 Field Measurements

Field data collection was conducted right after UAS-SfM photogrammetric survey for all dates (06/01/2022, 06/16/2022, 07/15/2022) To collect manual height measurements, a meter scale was utilized, ensuring that the measurements were consistent and accurate. Starting from the ground up to the tassel of the plant. Figure 3.5 illustrates where the height was measured to.

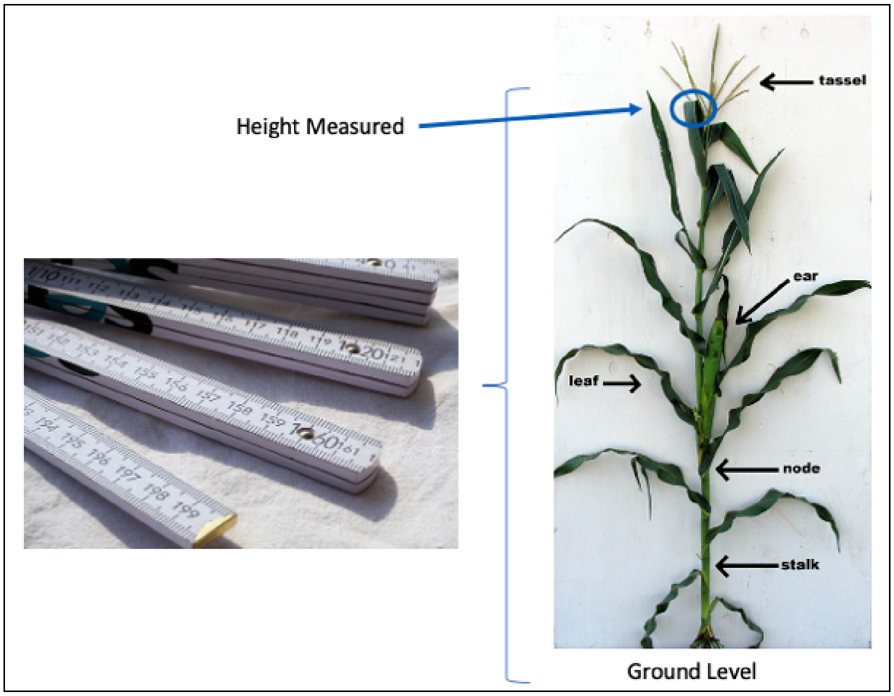

Figure 3.5
Illustration of a corn plant, highlighting its various parts. The image indicates the measurement of plant height from the ground to the tassel, demonstrating the standardized methodology employed for manual height measurement in the study.

Data collection was conducted from 36 distinct sections within the 3rd planting field, as shown in figure 3.2. These sections, each spanning 0.8 meters in width and 1 meter in length, served as the source for plant height measurements. The field was organized into a layout that featured four repeated rows, and in adherence to this pattern, manual measurements were taken at intervals of four rows. Within each section, every plant was measured, with the number of plants per section ranging between 6 and 12. The criteria for section selection stipulated that only those containing at least six plants within a 1-meter distance were chosen. To uphold the authenticity and dependability of the collected field data, measurements were not taken from border plots. This precaution was taken to reduce possible biases due to edge effects, which could potentially compromise the precision and applicability of the results.

CHAPTER 4: METHODOLOGY

4.1 Georeferencing Systems Comparison

A graphical representation of different positioning systems is shown in figure 4.6. Standalone (uncorrected) GNSS measurements were made during flight by the receiver onboard the UAS platform; RTK corrected GNSS measurements were made during flight using the DJI D-RTK 2 local GNSS base station; and RTK corrected GNSS measurements were made during flight using RTN correction service of continuously operating GNSS reference stations provided by TxDOT as opposed to a local base station. This comparison aimed to investigate the accuracy and efficiency of these georeferencing methods in the context of UAS-SfM photogrammetry for crop height measurement and monitoring. By comparing the performance of GNSS-only, GNSS+RTK from DJI D-RTK 2, and GNSS+RTN from TxDOT, the study sought to determine the most suitable and accurate georeferencing techniques dependent on accuracy and precision needs.

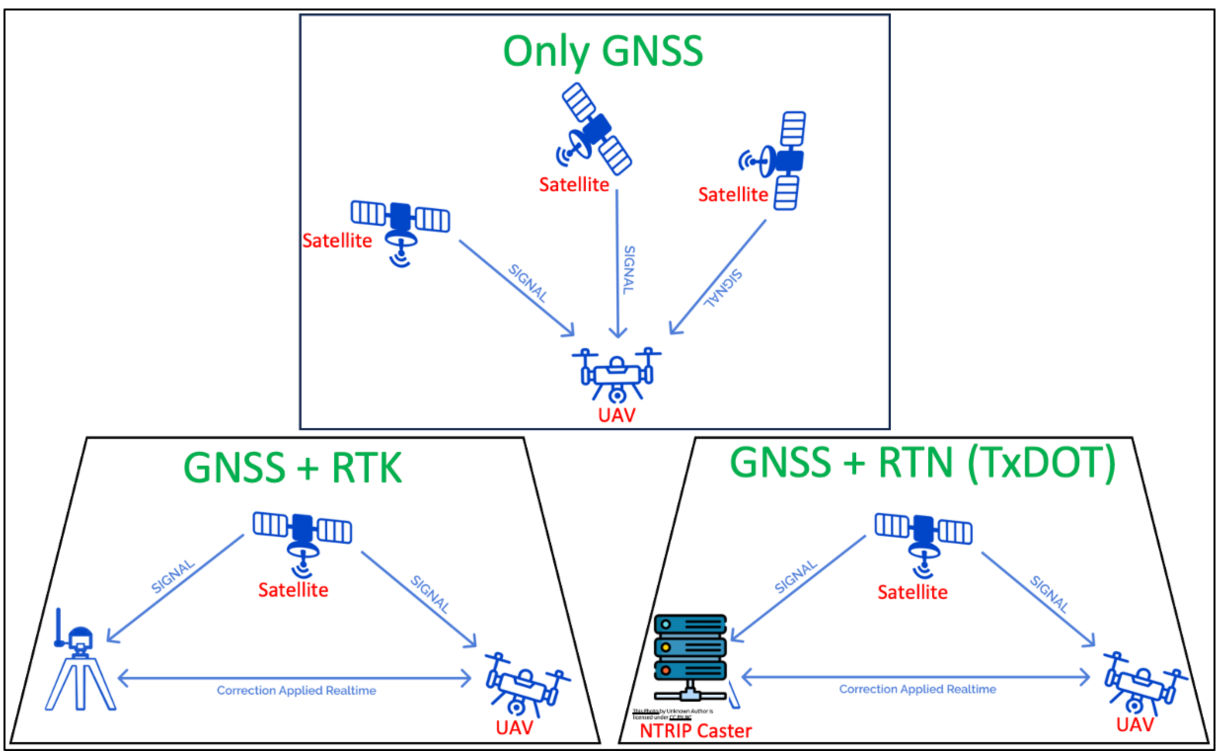

Figure 4.6
Graphical representation of different positioning systems, including GNSS-only, GNSS+RTK corrections, and GNSS+RTN.

The Emlid Reach RS2 GNSS receiver was utilized to survey GCPs. It is a high-precision GNSS receiver capable of providing centimeter-level accuracy, making it a useful tool for surveying GCPs in support of UAS survey projects. The use of this equipment facilitated the collection of high-quality geolocation data, which served as a reference for assessing the accuracy and performance of the three georeferencing systems under investigation. A total of 9 GCPs were strategically placed within the study area to provide accurate and reliable geolocation data for the subsequent analysis and comparison of the georeferencing systems. The selection of GCPs and checkpoints for the georeferencing systems comparison study is demonstrated in figure 4.7.

Figure 4.7
Aerial view of the field showcasing the strategic placement of GCPs and checkpoints. The image provides a clear depiction of the spatial distribution of these critical points across the study area.

The distribution pattern of the 9 GCPs in the field was strategically designed to optimize both the accuracy and the quality of the 3D reconstruction. The number of GCPs selected varied depending on the experiment, with either 1 or 0 GCPs selected as 3D GCP, and either 8 or 9 GCPs selected as checkpoints for the georeferencing experiment. In the scenarios where 1 GCP was selected as 3D GCP, this was located in the center of the field as shown in figure 4.7. The placement of a 3D GCP in the center of the field is a critical measure to enhance the quality of the reconstruction by mitigating systematic errors, such as the ”bowl effect”. This effect, often observed in photogrammetry, results from the accumulation of minor errors in the measurement of the camera lens model throughout the photogrammetric process. Checkpoints serve an important role in assessing the accuracy of the generated model by providing on-site, independently measured data against which the model's accuracy can be evaluated. They are an optional but highly recommended component of field setup for photogrammetric surveys, and their inclusion in this study further validates the resulting 3D models.

4.1.1 Standalone GNSS

During the first configuration of the study, the DJI Phantom 4 RTK drone was configured to fly and record the autonomous (uncorrected) GNSS measurements as opposed to utilizing RTK or another correction method during flight. This decision was made to examine the autonomous positional accuracy of the GNSS receiver onboard the UAS and assess its performance as a standalone method for georeferencing of camera/image positions and subsequent UAS-SfM data products. By focusing on autonomous GNSS measurements, the study aimed to establish a baseline for comparison with the differential GNSS georeferencing methods that incorporate RTK or RTN corrections.

4.1.2 GNSS+RTK

After assessing the GNSS-only georeferencing system, the DJI Phantom 4 RTK drone was configured to fly using GNSS combined with RTK corrections. The objective of this configuration was to evaluate the performance improvements offered by integrating RTK corrections into the georeferencing process. By incorporating RTK corrections, the study aimed to determine the extent to which this advanced georeferencing method could enhance the quality and accuracy of UAS-SfM data acquisition and analysis when compared to autonomous GNSS (GNSS-only).

The RTK corrections for precise georeferencing were received from a DJI D-RTK 2 local GNSS base station, enhancing the accuracy of the UAS-SfM survey. This technique required the acquisition of an accurate base position coordinate, which was obtained by recording a Receiver Independent Exchange Format (RINEX) file for a period of eight hours. The recording was conducted using the Emlid Reach RS2 GNSS receiver. After obtaining the RINEX file, the collected RINEX file was uploaded to the Online Positioning User Service (OPUS), a free online service provided by the National Geodetic Survey. OPUS uses data from a network of permanent GNSS stations to provide corrected coordinates for the uploaded file's location. After the upload, OPUS processed the RINEX data and delivered the precise base position coordinate. This base position coordinate was then configured in the GNSS+RTK base station. During the UAS flights, the base station transmitted correction data to the drone in real-time, leveraging the RTK method. This enabled the drone to apply corrections to its GNSS data, significantly enhancing the spatial accuracy of the acquired images. This process substantially reduced post-processing time.

4.1.3 GNSS+RTN

In the final configuration of the study, the DJI Phantom 4 RTK drone was set to fly using GNSS combined with TxDOT RTN network corrections. The goal of this configuration was to explore the performance improvements achieved by incorporating RTN corrections during flight into the georeferencing process as opposed to using a local base station. By integrating TxDOT RTN corrections with the GNSS system, the study sought to assess the extent to which this advanced georeferencing method could further enhance the quality and accuracy of UAS-based data acquisition and analysis in comparison to the GNSS-only and GNSS+RTK systems. This comparison not only emphasized the advantages of employing GNSS+RTN corrections but also offered valuable insights to optimize data collection and processing workflows using the most advanced and efficient georeferencing methods available.

To facilitate the reception of TxDOT RTN corrections by the DJI Phantom 4 RTK drone, a Wi-Fi network generated from a mobile hotspot was employed for the DJI remote controller. This approach allowed for seamless data transmission between the RTN caster and the drone's remote controller, ensuring that the drone could consistently receive real-time corrections during the flight. The credentials required to access the RTN service were provided by TxDOT, ensuring that the study utilized a reliable and well-maintained source of correction data. Leveraging this mobile hotspot setup allowed to effectively assess the performance of the GNSS+RTN georeferencing system under real-world conditions.

4.2 Plant Height Estimation

For the plant height estimation study, a total of 9 GCPs were strategically placed within the study area to provide accurate and reliable geolocation data for the subsequent analysis and comparison of the georeferencing systems. The selection of GCPs and checkpoints for the plant height study is demonstrated in figure 4.8.

Figure 4.8
Aerial view of the field showcasing the strategic placement of GCPs and checkpoints. The image provides a clear depiction of the spatial distribution of these critical points across the study area.

Five of these points were used as 3D GCPs, one placed at each corner of the field and one in the middle. The corner placement of the 3D GCPs is a common practice to provide a frame of reference that covers the entire area of interest, ensuring accurate geolocation across the whole field. The remaining four GCPs were positioned along the edges of the field and designated as checkpoints.

4.3 SfM Data Processing

The image sets acquired from each UAS flight and respective GNSS method (GNSS-only, GNSS+RTK, GNSS+RTN) applied for georeferencing of the image locations were imported into the commercial SfM photogrammetry software, PIX4Dmapper, to process and generate geospatial data products for subsequent analysis, including estimation of canopy height. A description of the photogrammetric data processing workflow implemented within the PIX4Dmapper software is provided below.

4.3.1 Georeferencing Studies

4.3.1.1 Import Imagery

The image sets acquired with corrections from GNSS methods (uncorrected, RTK, RTN) were imported into the PIX4Dmapper SfM photogrammetry software to process and generate geospatial data, based on the geotag locations. Once the images have been successfully imported, PIX4Dmapper automatically parses the embedded geolocation and orientation metadata, which will be utilized in subsequent processing steps.

To ensure consistent and accurate georeferencing throughout the project, users must configure the coordinate system and geolocation accuracy settings within PIX4Dmapper. When analyzing the imagery dataset from uncorrected GNSS and GNSS+RTK, the World Geodetic System 1984 (WGS 1984) datum was selected as the geographic coordinate system which is the global reference system used by the GNSS measurements recorded by the receiver onboard the UAS. On the other hand, when analyzing the imagery dataset from GNSS+RTN, the NAD83 National Spatial Reference System 2011 (NAD83 2011) datum was selected as the geographic coordinate system which is the reference system used by TxDOT RTN. Additionally, the geolocation accuracy was set to "Standard," which balances processing time with the level of precision required for most applications. Once these settings were configured, PIX4Dmapper automatically detected the camera model used to capture the raw imagery, in this case, the FC6360. This step is crucial for ensuring that the software correctly interprets and processes the image data, accounting for the unique characteristics and specifications of the camera sensor used in the drone.

4.3.1.2 Photo Alignment & Calibration

After importing the raw images into PIX4Dmapper, the calibration and estimation of the camera exterior orientations (position and orientation of the camera at the time each photo was acquired) was initiated. The following is the configuration selected from the Initial Processing menu. The custom option with 1 (original image size) was selected for keypoints image scale, which allowed for a more accurate alignment by retaining the original image resolution. The aerial grid or corridor was chosen as the option for matching image pairs, and geometrically verified matching was used to improve the accuracy of the results. The targeted number of keypoints was set to automatic, which determined the number of keypoints based on the number of images and the image content. To ensure accurate geolocation and orientation, the calibration method was set to 'accurate geolocation and orientation', and the rematch option was selected to further refine the alignment if necessary. These parameters were specifically selected to obtain a high-quality alignment that would facilitate the generation of accurate georeferenced data.

4.3.1.3 Import GCPs & Re-optimize

During the GCP importing process in PIX4Dmapper, the WGS 84 geographic coordinate system was selected. A complete summary of the GCP placement for the georeferencing experiment is shown in table 4.2. Once the GCPs were imported, the GCP tagging process began to locate the center of the GCP in the image. This process involved identifying and marking the GCPs on each image, which allowed for precise georeferencing during the point cloud and mesh generation process. After GCP tagging, the reoptimize process was performed, which re-adjusted the position and orientation of the camera to improve the accuracy of the results.

Table 4.2
Experiement GCP placement setting.

UAS Flight Date	**Number of GCPs & Type**	**GNSS Receiver**
06/01/2022	8 Checkpoints; 1 3D GCP	GNSS+RTK
06/01/2022	9 Checkpoints; 0 3D GCP	GNSS+RTK
06/01/2022	8 Checkpoints; 1 3D GCP	Uncorrected GNSS
06/01/2022	9 Checkpoints; 0 3D GCP	Uncorrected GNSS
06/16/2022	8 Checkpoints; 1 3D GCP	GNSS+RTK
06/16/2022	9 Checkpoints; 0 3D GCP	GNSS+RTK
06/16/2022	8 Checkpoints; 1 3D GCP	GNSS+RTN
06/16/2022	9 Checkpoints; 0 3D GCP	GNSS+RTN
06/16/2022	8 Checkpoints; 1 3D GCP	Uncorrected GNSS
06/16/2022	9 Checkpoints; 0 3D GCP	Uncorrected GNSS
07/15/2022	8 Checkpoints; 1 3D GCP	GNSS+RTK
07/15/2022	9 Checkpoints; 0 3D GCP	GNSS+RTK
07/15/2022	8 Checkpoints; 1 3D GCP	GNSS+RTN
07/15/2022	9 Checkpoints; 0 3D GCP	GNSS+RTN
07/15/2022	8 Checkpoints; 1 3D GCP	Uncorrected GNSS
07/15/2022	9 Checkpoints; 0 3D GCP	Uncorrected GNSS

4.3.1.4 Generate Quality Report

One of the essential outputs generated by the software is a comprehensive quality report, which provides an overview of the project's accuracy and quality metrics. For this study, the primary focus was on the results presented in the geolocation details section of the report, specifically about the GCPs. Therefore, in this particular case, neither the orthorectified orthomosaic nor the DSM were generated.

The geolocation details section of the report contains essential information about the accuracy and precision of the GCPs used during the project. These metrics are crucial for evaluating the overall accuracy of the 3D reconstruction (densified point cloud) of the imaged scene, which directly impacts the quality of the generated orthomosaics, DSMs, and DTMs. In this study, the main focus was on the values for Root Mean Square Error (RMSE) for X, Y, and Z coordinates. The RMSE represents the average difference between the true and estimated values for each coordinate, with lower values indicating a higher level of accuracy. The formula to calculate RMSE is $\mathrm{RMSE}(x,\hat{x}) = \sqrt{\frac{\sum_{i=1}^{N}(x_i-\hat{x}_i)^2}{N}}$ where N is the number of data points, x_i is the i-th measurement, and $\hat{x}_i$ is its corresponding prediction.

4.3.2 Plant Height Studies

4.3.2.1 Import Imagery

The image sets acquired with corrections only from GNSS+RTK method, were imported into the PIX4Dmapper SfM photogrammetry software to process and generate geospatial data based on the geotag locations. Once the images have been successfully imported, PIX4Dmapper automatically parses the embedded geolocation and orientation metadata, which will be utilized in subsequent processing steps.

To ensure consistent and accurate georeferencing throughout the project, users must configure the coordinate system and geolocation accuracy settings within PIX4Dmapper. For this study, the World Geodetic System 1984 (WGS 1984) datum was selected as the geographic coordinate system, which is the global reference system used by the GNSS measurements recorded by the receiver onboard the UAS. Additionally, the geolocation accuracy was set to ”Standard,” which balances processing time with the level of precision required for most applications. Once these settings were configured, PIX4Dmapper automatically detected the camera model used to capture the raw imagery, in this case, the FC6360. This step is crucial for ensuring that the software correctly interprets and processes the image data, accounting for the unique characteristics and specifications of the camera sensor used in the drone.

4.3.2.2 Photo Alignment & Calibration

After importing the raw images into PIX4Dmapper, the next step was to align the photos. In the alignment process, the full option was selected for the keypoints image scale, which allows for the detection of keypoints in the full-resolution images. The aerial grid or corridor option was selected for the matching image pairs, which optimizes the matching process for aerial images taken in a grid or corridor flight pattern. The targeted number of keypoints was set to automatic, which allows the software to automatically adjust the number of keypoints based on the image content and quality. Finally, the calibration method was set to standard, which uses a mathematical model to correct for lens distortion and calibrate the camera parameters. The alignment process is critical to ensure accurate orthomosaic and DSM generation, which is necessary for obtaining accurate estimates of plant height from the images.

4.3.2.3 Import GCPs & Re-optimize

To improve the accuracy of the georeferencing process, GCPs were imported into PIX4Dmapper. The GCPs were collected on the field using the Emlid Reach RS2 receiver. WGS 84 was selected as the GCP coordinate system in PIX4Dmapper, which matched the coordinate system used by the Emlid Reach RS2. A total of five GCPs were selected as 3D GCPs, while four GCPs were selected as checkpoints to validate the accuracy of the processing. Once the GCPs were imported into PIX4Dmapper, the GCP tagging process began to locate the center of the GCP in the images. This process involved manually placing a marker on the center of the cross of each GCP in each image in which it was visible. By using GCPs, the software can adjust the positioning and orientation of the images, which helps to improve the accuracy of the final output.

4.3.2.4 Point Cloud and Mesh

Once the photos were aligned and GCPs imported in PIX4Dmapper, the point cloud and mesh generation process was initiated. For the point cloud, image scale option of 1 (original image size) with multiscale enabled was selected. This option allows the creation of a dense and accurate point cloud. Then, the point density was set to optimal and selected a minimum of 3 matches. This ensured that the point density and processing time were balanced to obtain a satisfactory point cloud. Following the point cloud generation, the mesh was created using the medium resolution setting in the 3D textured mesh options. This setting produced a mesh with a reasonable number of triangles while maintaining an adequate level of detail. The point cloud generated in the previous step was used for mesh generation. Selecting these specific parameters allowed to generate a high-quality mesh that accurately represented the topography and vegetation structure of the study area.

4.3.2.5 Generate DSM, DTM, and Orthomosaic

After the point cloud and mesh generation, the next step was the generation of the DSM and orthomosaic in PIX4Dmapper. The resolution was set to 5 cm/pixel ensuring that both the DTM and DSM had the same resolution. During the generation process, to improve the quality of the output, the options to use noise filtering and surface smoothing were selected. Additionally, sharp was selected as the DSM filter type, which is a suitable filter type for agricultural areas with sharp changes in height. The method used to raster the DSM was inverse distance weighting, which assigns weights to neighboring points to estimate the height at a specific location.

In this study, the DTM was generated using three different methods to evaluate their effectiveness and accuracy creating a more reliable representation of the ground surface, which is crucial for generating accurate CHMs. The first method involved utilizing the automatic classification tool from PIX4Dmapper, which generated the DTM with the same resolution as the DSM. The point cloud classification tool was employed to improve the DTM generation process by classifying ground points, thereby facilitating the accurate identification of the terrain and the creation of a reliable DTM. The second method for generating the DTM involved using the Triangulated Irregular

Network (TIN) interpolation tool available in QGIS. This approach allowed for the construction of a surface model by connecting adjacent ground elevation points that were selected manually all over the field, resulting in a detailed and accurate representation of the ground surface. The third method of generating the DTM was based on using elevation data from a flight conducted before plant emergence. This approach leveraged existing elevation data, for representing the ground surface on the terrain model.

With the DSM and DTM generated, the next step was the orthomosaic generation process. The orthomosaic is a geometrically corrected aerial image that has been adjusted to have a uniform scale, so distances can be measured directly from it. To ensure consistency throughout the analysis, the orthomosaic was set to have the same resolution as the DSM and DTM

4.3.3 Generate CHM

To generate the CHM, DSM was subtracted from the DTM using the raster calculator tool in QGIS. Since both the DSM and DTM had the same resolution, the resolution was preserved for the generated CHM. This ensured that the spatial consistency and accuracy of the analysis were maintained. For the purpose of this research, the output Coordinate Reference System (CRS) used was EPSG:32614 - WGS 84 / UTM zone 14N, which facilitated data integration with other spatial datasets within the study area.

4.3.4 Obtain Plant Height

In this study, the Zonal Statistics tool in QGIS was utilized to calculate the maximum height of plants from the CHM within the designated plot boundaries. This tool operates by overlaying the vector geometries (i.e., the plot boundaries) onto the raster dataset (i.e., the CHM) and computing the desired statistics (in this case, the maximum height) for each zone or plot.

4.3.5 Generate Canopy Cover

To implement the Canopeo method using QGIS, the orthomosaic images were first imported into QGIS. In this case, the Raster Calculator was used to apply a color-based segmentation formula to separate green vegetation pixels from the background. The formula,

$$((\text{Red}/\text{Green}) < 0.95\ AND\ (\text{Blue}/\text{Green}) < 0.95\ AND\ (2 * \text{Green} - \text{Red} - \text{Blue}) > 20)$$

is designed to emphasize the greenness of vegetation and minimize the influence of other colors, allowing for a more accurate estimation of canopy cover. This workflow is shown in figure 4.9.

By applying this formula within the Raster Calculator tool, a new raster layer was generated that highlights the areas of green vegetation in the orthomosaic images. This layer can then be used to calculate the fractional green canopy cover by determining the ratio of green vegetation pixels to the total number of pixels within the defined area of interest.

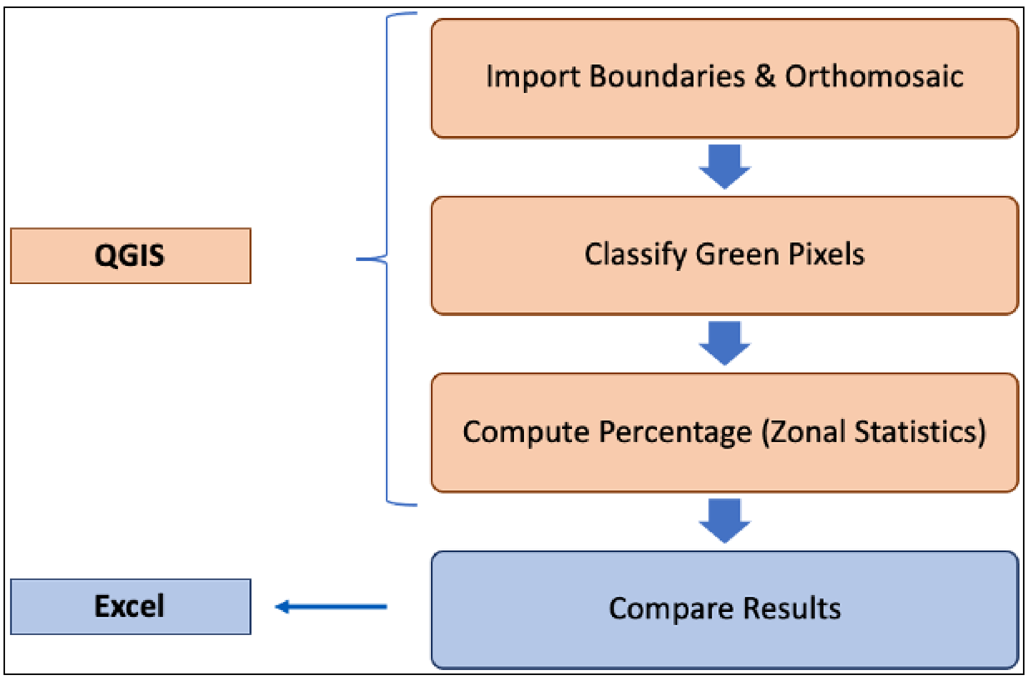

Figure 4.9
Illustration of the UAS green canopy cover estimation workflow. The image provides a step-by-step visual guide of the process, from initial pixel classification to final percentage cover computation.

4.4 Comparative Accuracy Assessment

For further analysis, the next step was a detailed comparison of the accuracy in both the horizontal (X, Y) direction and the vertical (Z) direction. This values can be obtained from a report generated from Pix4Dmapper. An example of this report is shown in figure 4.10.

Bar charts were computed to present the RMSE values in a visual format for the X, Y, and Z coordinate components for each GNSS method and UAS flight. The effectiveness of the different georeferencing methods could be determined from the visual and quantitative RMS results, thereby allowing the selection of the most suitable approach for the study.

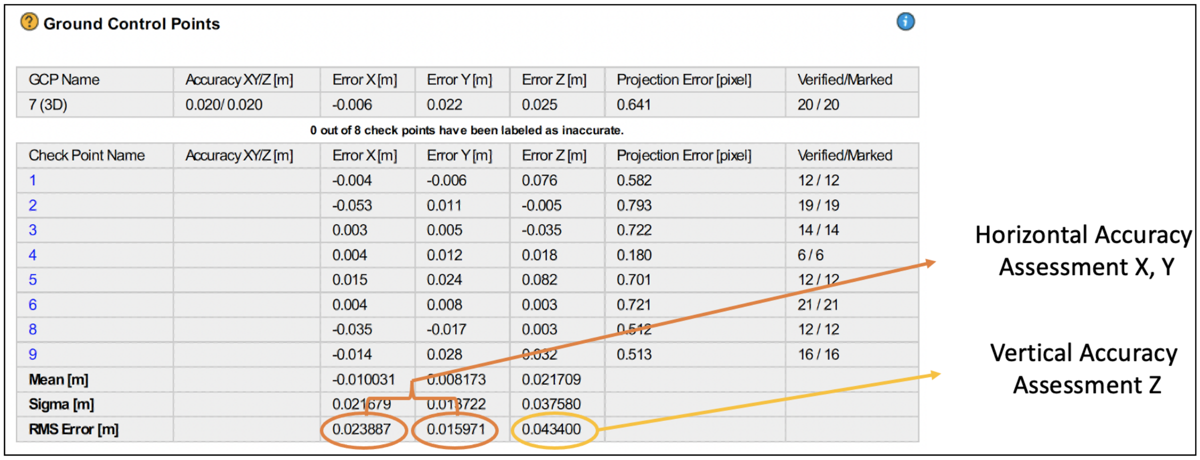

Ground Control Points

GCP Name	Accuracy XY/Z [m]	Error X [m]	Error Y [m]	Error Z [m]	Projection Error [pixel]	Verified/Marked
7 (3D)	0.020/ 0.020	-0.006	0.022	0.025	0.641	20 / 20

0 out of 8 check points have been labeled as inaccurate.

Check Point Name	Accuracy XY/Z [m]	Error X [m]	Error Y [m]	Error Z [m]	Projection Error [pixel]	Verified/Marked
1		-0.004	-0.006	0.076	0.582	12 / 12
2		-0.053	0.011	-0.005	0.793	19 / 19
3		0.003	0.005	-0.035	0.722	14 / 14
4		0.004	0.012	0.018	0.180	6 / 6
5		0.015	0.024	0.082	0.701	12 / 12
6		0.004	0.008	0.003	0.721	21 / 21
8		-0.035	-0.017	0.003	0.512	12 / 12
9		-0.014	0.028	0.032	0.513	16 / 16
Mean [m]		-0.010031	0.008173	0.021709		
Sigma [m]		0.021679	0.013722	0.037580		
RMS Error [m]		0.023887	0.015971	0.043400		

Figure 4.10
An example of report displaying the georeferencing errors for each checkpoint. The table provides a comprehensive breakdown of both horizontal and vertical inaccuracies, offering a quantitative assessment of geospatial accuracy in the study.

4.5 Estimating Plant Height from SfM

The generated geospatial data products output from Pix4Dmapper software, described above, were applied to estimate canopy height models for each UAS flight as described below. The workflow can be observed in figure 4.11.

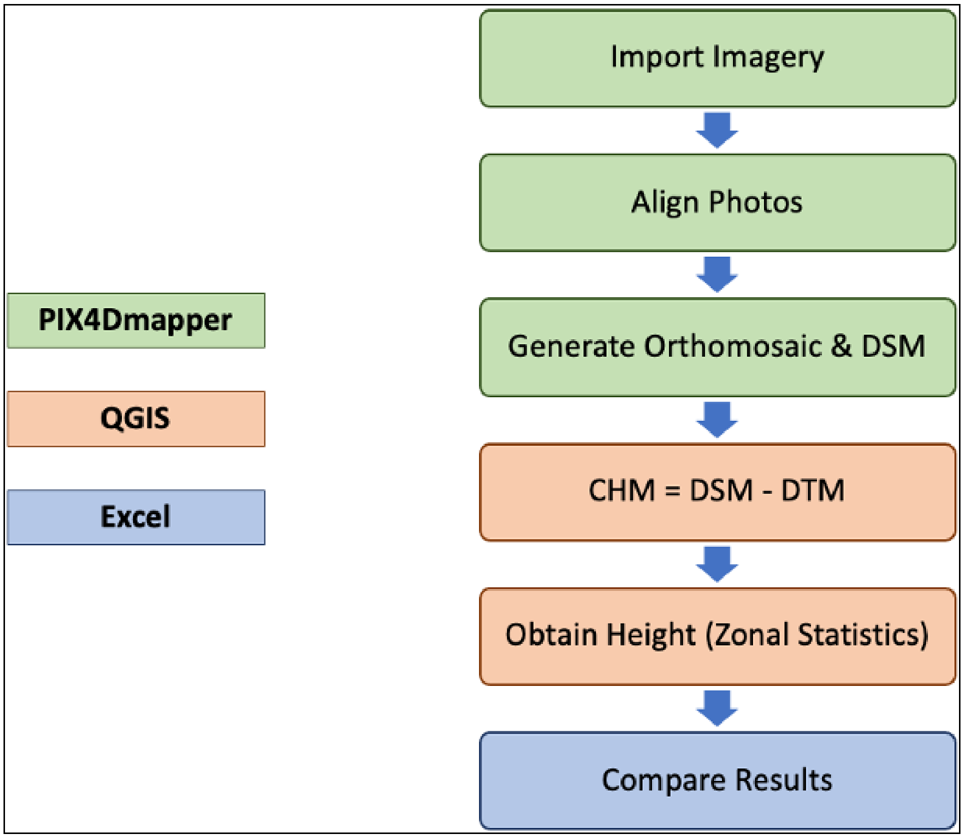

Figure 4.11
Illustration of the UAS derived plant height estimation workflow. The image provides a step-by-step visual guide of the process, from initial data acquisition to final height estimation and comparison.

With these outputs in hand, QGIS was employed to generate CHMs for every UAS flight date by subtracting the DTM from the DSM. Given that the DSMs and DTMs were generated at a resolution of 5 cm/pixel, the derived CHMs were also produced at the same resolution of 5 cm/pixel. Once the CHMs were generated, 36 plot boundaries of 0.8 meters in width and 1 meter in length were created to reduce the area containing ground and focus only on the area with plants. Example of these boundaries are shown in figure 4.12. The beginning and end of each boundary were surveyed using an Emlid Reach RS2 at the moment of manually measuring the plants in the field. Subsequently, the Zonal Statistics tool within QGIS was utilized to extract maximum height values from drawn plots.

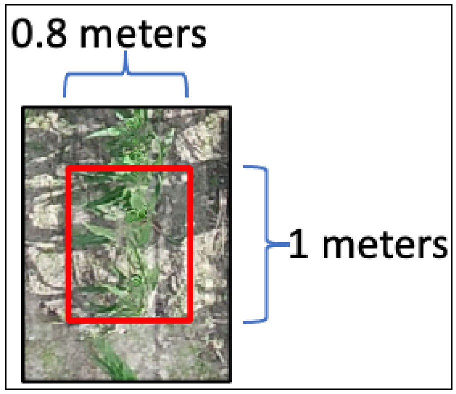

Figure 4.12
Schematic representation of plot boundaries, each measuring 0.8 meters in width and 1 meter in length, encircling the area of interest where plant heights were manually assessed.

4.5.1 Statistical Evaluation of UAS-SfM Plant Height Estimation Error

The relationship between the UAS-based crop canopy height estimates and ground-based measurements was obtained from calculating coefficient of determination (R^2).

CHAPTER 5: RESULTS & DISCUSSION

5.1 Georeferencing Systems Comparison

5.1.1 Results

Figures below show horizontal and vertical RMSE based on the PIX4Dmapper accuracy values provided in quality reports relative to checkpoints. These accuracy values report the difference in the result of the SfM bundle adjustment implemented in PIX4Dmapper to reconstruct the 3D target coordinate relative to the GCP coordinates surveyed using the ground-based methods.

Figures 5.13, 5.14, and 5.15, represent data collected on the 1st of June, 2022, using GNSS-only and GNSS+RTK. Best results were obtained when using GNSS+RTK from the DJI D-RTK 2 mobile station. Moreover, for horizontal accuracy assessment (X) and vertical accuracy assessment (Z), accuracy improved when using 1 GCP in comparison to not using any. In every scenario, the use of GNSS-only and no GCP reported the least accurate results.

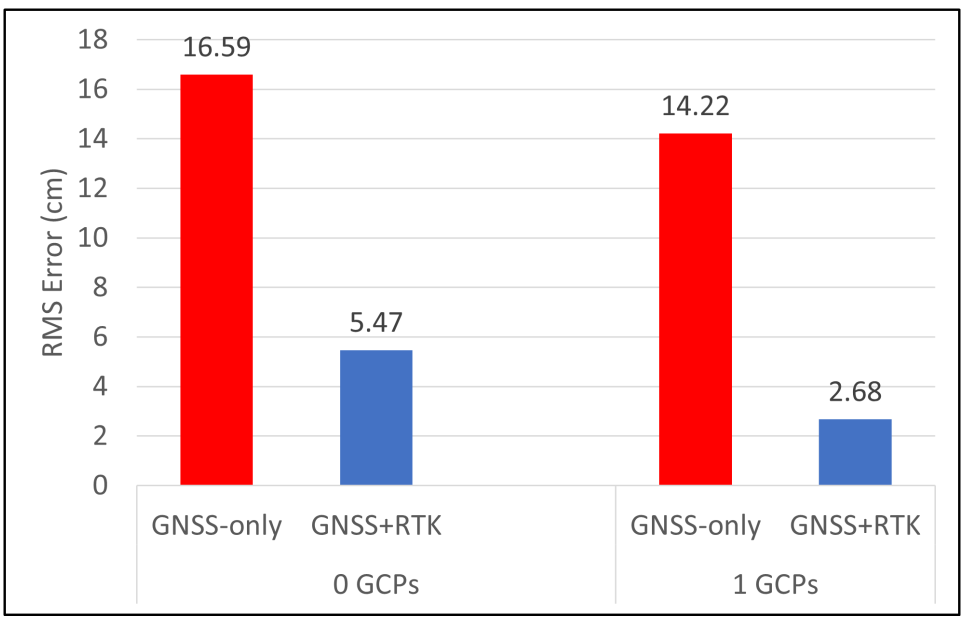

Figure 5.13
Horizontal accuracy (X) for 06/01/2022 comparing the RMSE measured in centimeters between GNSS-only and GNSS+RTK, considering different quantities of GCPs.

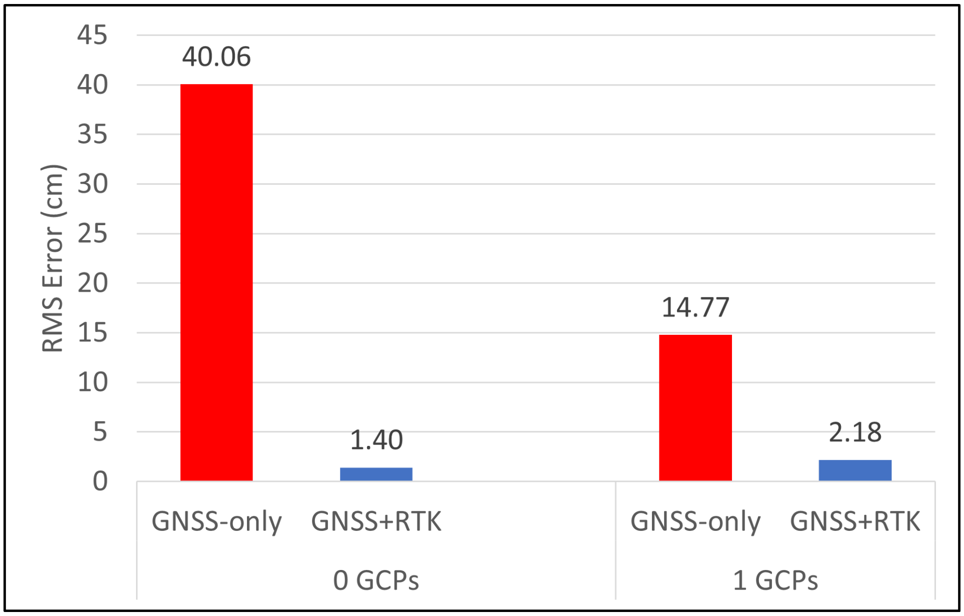

Figure 5.14
Horizontal accuracy (Y) for 06/01/2022 comparing the RMSE measured in centimeters between GNSS-only and GNSS+RTK, considering different quantities of GCPs.

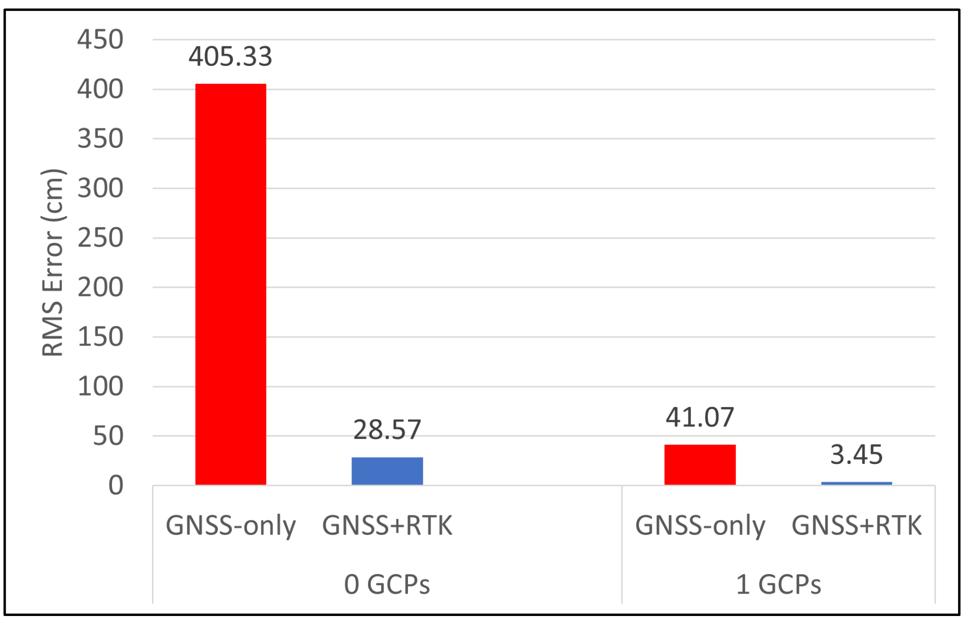

Figure 5.15
Vertical accuracy (Z) for 06/01/2022 comparing the RMSE measured in centimeters between GNSS-only and GNSS+RTK, considering different quantities of GCPs.

Figures 5.16, 5.17, and 5.18, represent data collected on the 16th of June, 2022, using GNSS-only, GNSS+RTK and GNSS+RTN. For horizontal accuracy assessment (X) and vertical accuracy assessment (Z), accuracy improved when using GNSS+RTK from the DJI D-RTK 2 mobile station. Moreover, the use of 1 GCP in GNSS-only corrections, significantly improved the results. In every scenario, the use of GNSS-only and no GCP reported the least accurate results.

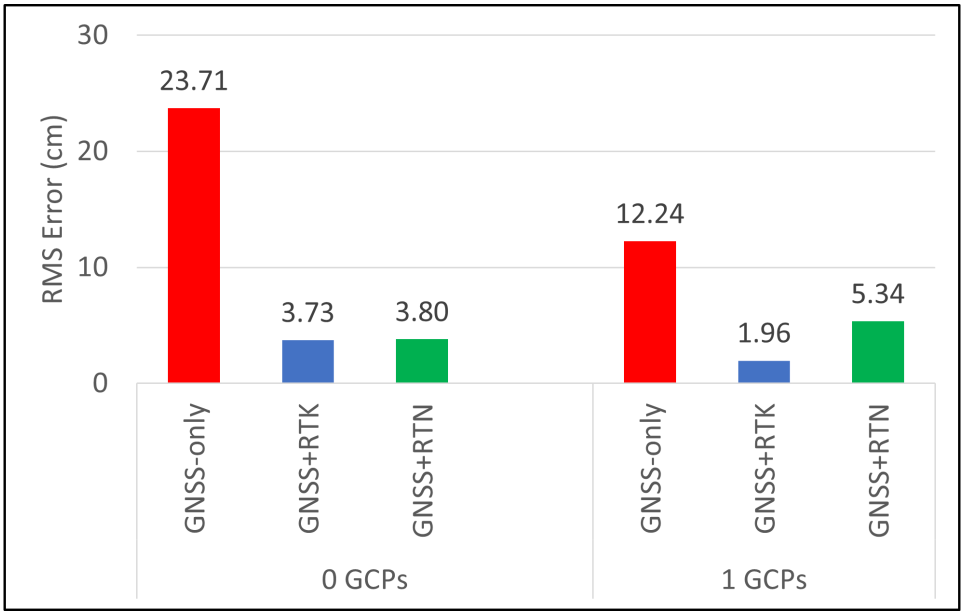

Figure 5.16
Horizontal accuracy (X) for 06/16/2022 comparing the RMSE measured in centimeters between GNSS-only, GNSS+RTK, and GNSS+RTN, considering different quantities of GCPs.

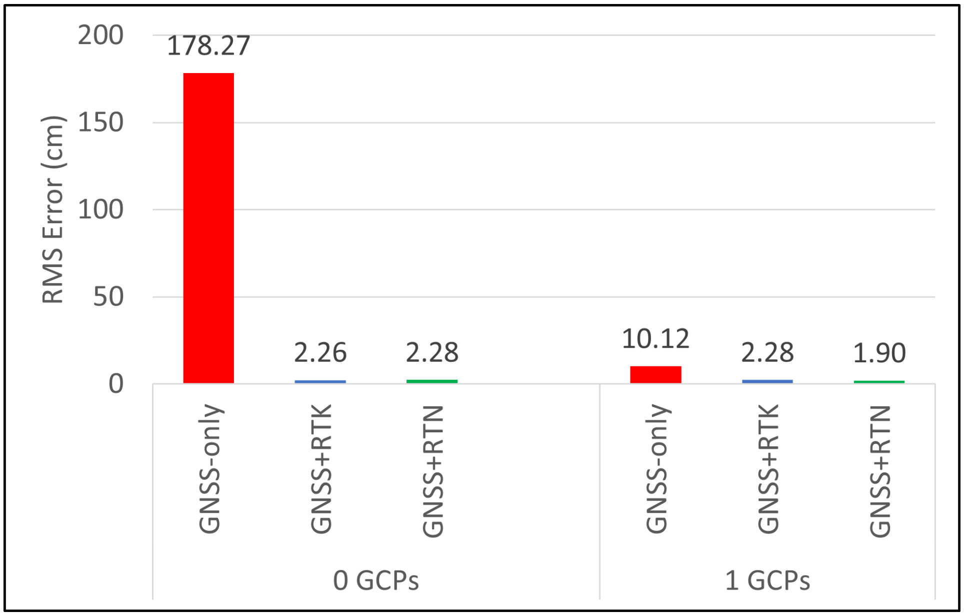

Figure 5.17
Horizontal accuracy (Y) for 06/16/2022 comparing the RMSE measured in centimeters between GNSS-only, GNSS+RTK, and GNSS+RTN, considering different quantities of GCPs.

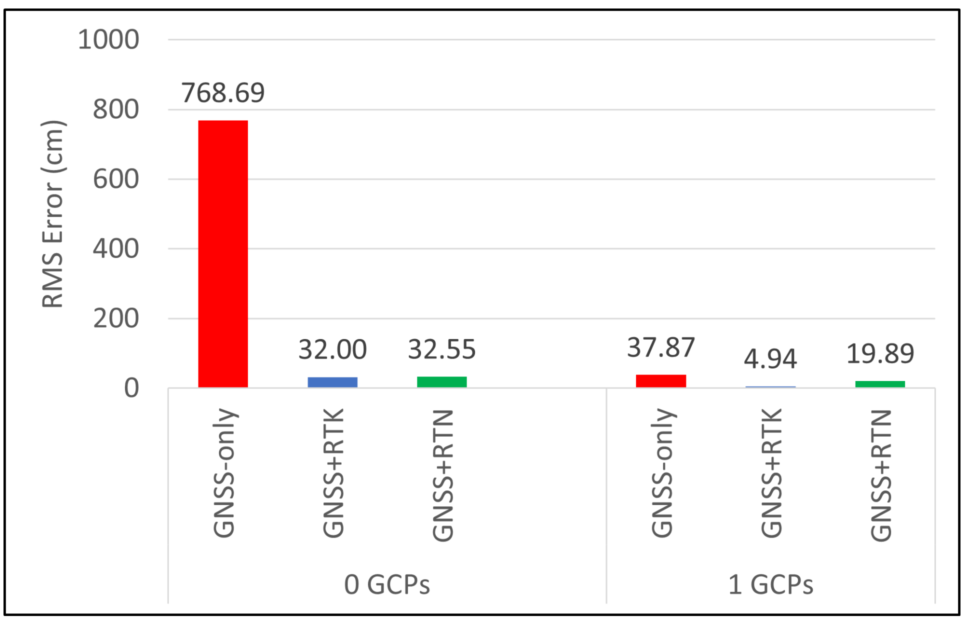

Figure 5.18
Vertical accuracy (Z) for 06/16/2022 comparing the RMSE measured in centimeters between GNSS-only, GNSS+RTK, and GNSS+RTN, considering different quantities of GCPs.

Figures 5.19, 5.20, and 5.21, represent data collected on the 15th of July, 2022, using GNSS-only, GNSS+RTK and GNSS+RTN. For all accuracy assessments, the use of 1 GCP in comparison to not using any, improves results in the different georeferencing methods. For horizontal accuracy assessment (X) and (Y), accuracy improved when using GNSS+RTK from the DJI D-RTK 2 mobile station. The sizeable error observed during the GNSS-only experiment for this date, may have been attributed to random error. In every scenario, the use of GNSS-only and no GCP reported the least accurate results.

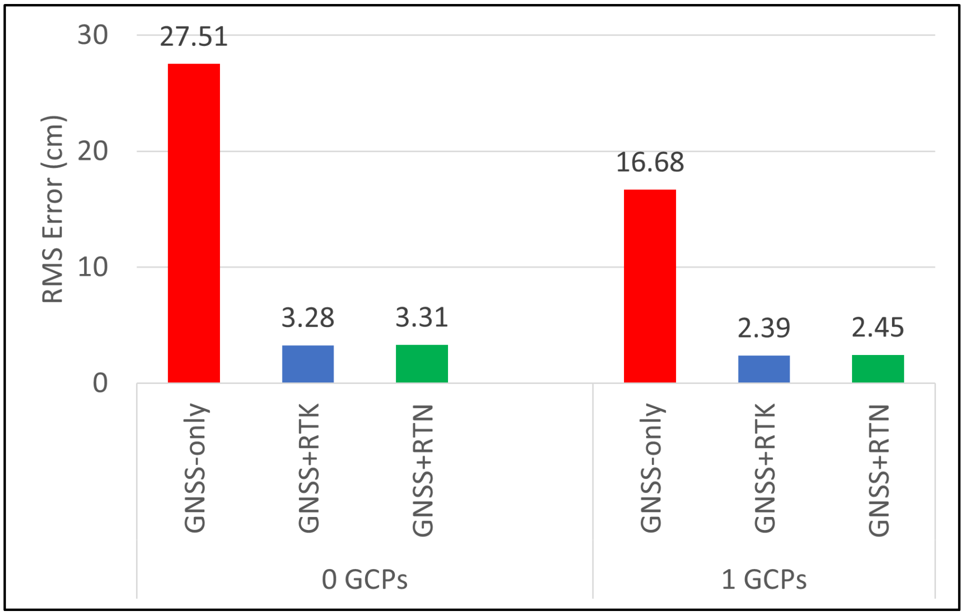

Figure 5.19
Horizontal accuracy (X) for 07/15/2022 comparing the RMSE measured in centimeters between GNSS-only, GNSS+RTK, and GNSS+RTN, considering different quantities of GCPs.

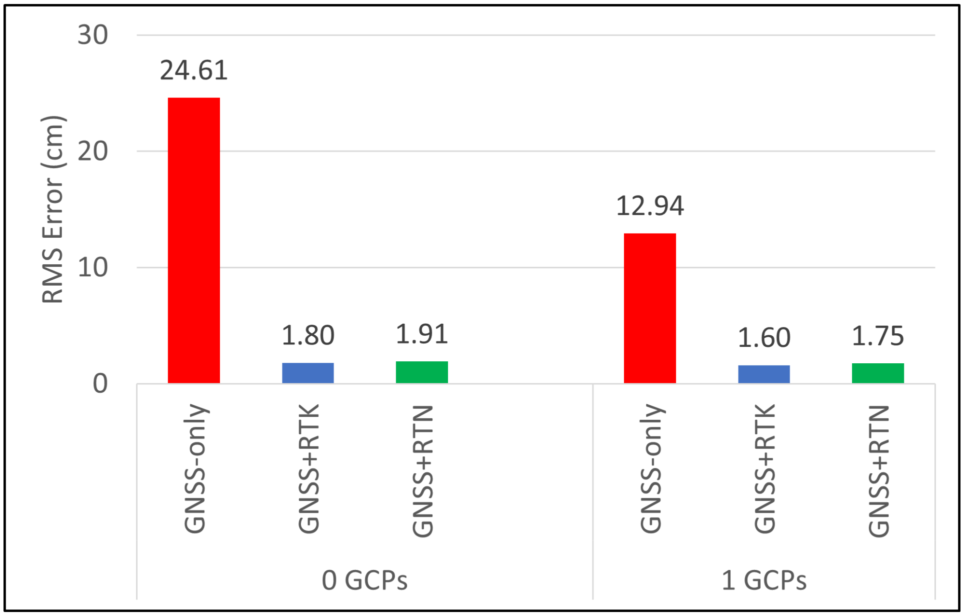

Figure 5.20
Horizontal accuracy (Y) for 07/15/2022 comparing the RMSE measured in centimeters between GNSS-only, GNSS+RTK, and GNSS+RTN, considering different quantities of GCPs.

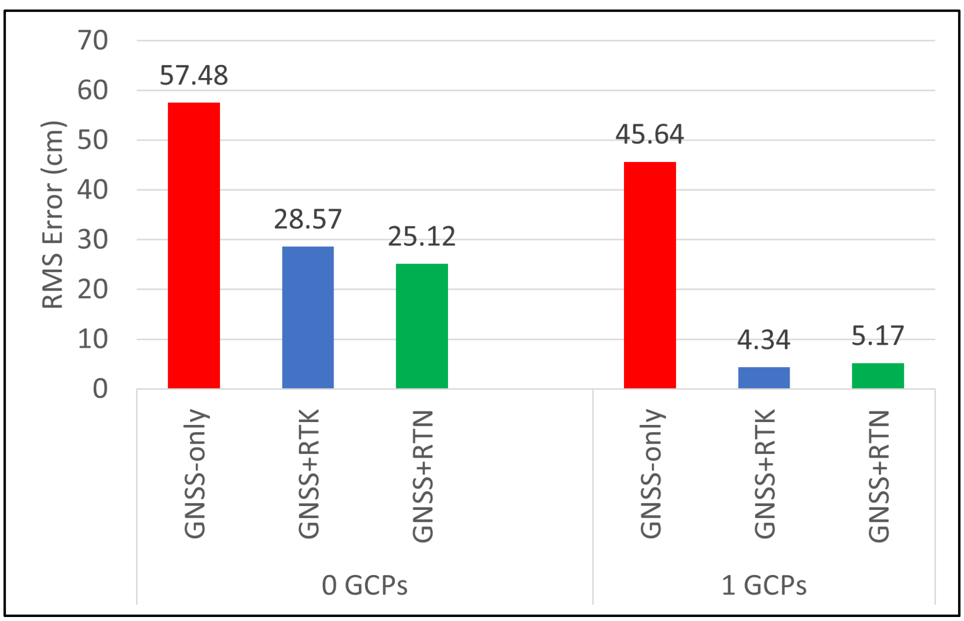

Figure 5.21
Vertical accuracy (Z) for 07/15/2022 comparing the RMSE measured in centimeters between GNSS-only, GNSS+RTK, and GNSS+RTN, considering different quantities of GCPs.

During analysis, an unforeseen discrepancy was encountered in vertical accuracy (Z) while employing the GNSS+RTK for geospatial data collection. This unexpected error estimation led us to revisit the methodology, prompting a resurvey of the reference points initially utilized for both, the DJI and the EMLID Reach base stations. The objective was to assess the discrepancy and attain more accurate measurements by comparing the original geospatial data—latitude, longitude, and ellipsoid height—with newly acquired geographical data derived from two different sources, namely OPUS processing services and TxDOT RTN. Findings revealed a substantial variation in the ellipsoid height measurements, with a difference of approximately 1.2 meters detected. This can be observed in table 5.3

Table 5.3
Comparative analysis showing significant discrepancy of approximately 1.2 meters in ellipsoid height measurements between the original data collected for both GNSS+RTK and EMLID Reach base stations and the new data derived from OPUS processing services and GNSS+RTK.

#	Use	Survey Eqpt	Latitude (dd)	Longitude (dd)	Ellipsoidal ht. (m)	Processing	Datum
1	Emlid RS2	V-MAP	27° 46’ 57.3204”	-97° 33’ 45.2694”	-11.407	-	NAD83(2011)
1	Emlid RS2	EMLID RS2	27° 46’ 57.3234”	-97° 33’ 45.2592”	-10.156	OPUS	NAD83(2011)
1	Emlid RS2	TxDOT	27° 46’ 57.3234”	-97° 33’ 45.2556”	-10.155	-	NAD83(2011)
Diff.	-	-	-	-	-1.251	-	-
2	GNSS+RTK	V-MAP	27° 46’ 57.4962”	-97° 33’ 45.7236”	-11.506	-	NAD83(2011)
2	GNSS+RTK	EMLID RS2	27° 46’ 57.4998”	-97° 33’ 45.7122”	-10.218	OPUS	NAD83(2011)
2	GNSS+RTK	TxDOT	27° 46’ 57.4998”	-97° 33’ 45.7122”	-10.192	-	NAD83(2011)
Diff.	-	-	-	-	-1.288	-	-

The accuracy of the UAS imagery data and surveying GCPs using GNSS+RTK and the EMLID RS2 receiver was challenged by a height error of approximately 1.2 meters. Interestingly, both systems exhibited a similar level of error, thus placing the measurements on a commensurate scale. However, further inspection uncovered an additional discrepancy: the height of the GNSS+RTK rod was off by 1.802 meters.

To identify the source of these errors, a thorough investigation was conducted. This examination led to the realization that an essential factor had been initially overlooked: the height of the RTK collector above the ground when using the GNSS+RTK base station. This height is determined by adding the distance from the top of the rod to the phase center to the total rod length as shown in figure 5.22. Given that the measurement of the GNSS base station receiver is taken at the phase center in the antenna, a correction of subtracting 1.802 meters from the original point was necessary.

Informed by this revelation, the RTK coordinate offset was adjusted accordingly. Following this correction, a new UAS imagery survey was executed on the subsequent flight date of April 11, 2023 specifically for the vertical accuracy assessment. This experience underscored the critical importance of rigorous attention to detail, particularly in the setup and calibration of RTK systems, to ensure data precision.

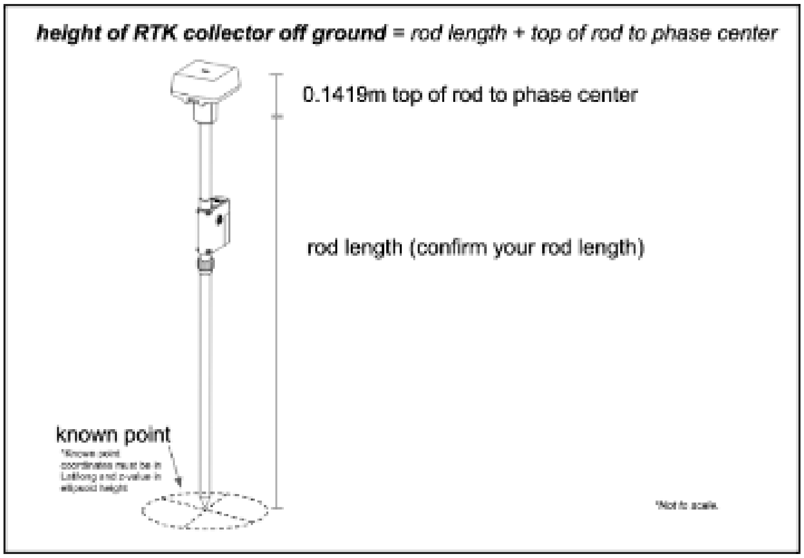

Figure 5.22
Detailed illustration of the DJI D-RTK 2 collector, showing the rod length and the measurement from the top of the rod to the phase center. The image illustrates the key components that constitute the total height of the RTK collector, a critical parameter in enhancing geospatial accuracy.

In figure 5.23, for data collected on the 11th of April, 2023, best results were obtained when using 1 GCP in comparison to not using any.

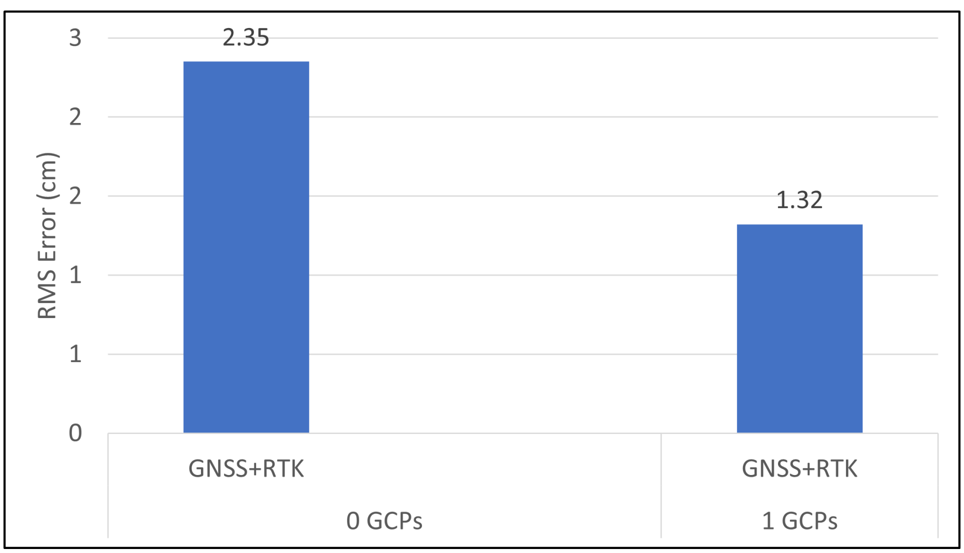

Figure 5.23
Vertical accuracy (Z) for 04/11/2023 comparing the RMSE measured in centimeters between GNSS+RTK considering different quantities of GCPs.

The study carried out a comprehensive analysis of the RMSE for X, Y, and Z coordinates for each GNSS georeferencing method across four distinct flight dates. These methods included GNSS-only, GNSS+RTK, and GNSS+RTN. A summary for all data collected is shown in table 5.4.

Table 5.4
Summary of RMSE for X, Y, and Z coordinates for each GNSS method.

Date	Georeferencing	GCPs	Acc. X (cm)	Acc. Y (cm)	Acc. Z (cm)
6/1/2022	GNSS-only	0	16.59	40.06	405.33
6/1/2022	GNSS-only	1	14.22	14.77	41.07
6/1/2022	GNSS+RTK	0	5.47	1.4	28.57
6/1/2022	GNSS+RTK	1	2.68	2.18	3.45
6/16/2023	GNSS-only	0	23.71	178.27	768.69
6/16/2023	GNSS-only	1	12.24	10.12	37.87
6/16/2023	GNSS+RTK	0	3.73	2.26	32
6/16/2023	GNSS+RTK	1	1.96	2.28	4.94
6/16/2023	GNSS+RTN	0	3.8	2.28	32.55
6/16/2023	GNSS+RTN	1	5.34	1.9	19.89
7/15/2023	GNSS-only	0	27.51	24.61	57.48
7/15/2023	GNSS-only	1	16.68	12.94	45.64
7/15/2023	GNSS+RTK	0	3.28	1.8	28.57
7/15/2023	GNSS+RTK	1	2.39	1.6	4.34
7/15/2023	GNSS+RTN	0	3.31	1.91	25.12
7/15/2023	GNSS+RTN	1	2.45	1.75	5.17
4/11/2023	GNSS+RTK	0	-	-	2.35
4/11/2023	GNSS+RTK	1	-	-	1.32

The table presents a detailed comparison of the accuracy achieved by different georeferencing methods - GNSS-only, GNSS+RTK, and GNSS+RTN - across various dates. These comparisons consider assessments of horizontal accuracy (X and Y coordinates) and vertical accuracy (Z coordinate).

For most of the results, the accuracy of checkpoints, in this case reported as RMSE (cm), was inversively proportional to the number of GCPs been used. Moreover, comparing vertical accuracy 0 GCPs vs 1 GCP, the use of 1 GCP substantially decreases the error. It is for this reason that for the second objective of this research, GNSS+RTK was utilized as the source for correction from common errors in satellite navigation systems. For the flight dates of 06/16/2022 and 07/15/2022, all three georeferencing methods were implemented and tested. Among all the assessments conducted, GNSS+RTK demonstrated superior performance in 80% of the tests when compared to the other two methods. Moreover, it yielded the most accurate results for the vertical accuracy assessment Z (cm). On the flight date of 06/01/2022, only two georeferencing methods, namely GNSS-only and GNSS+RTK, were tested. In all assessments conducted on this date, GNSS+RTK performed better than GNSS-only. Lastly, for the data collected on 04/11/2023, only GNSS+RTK was used. This followed a correction in the RTK coordinate offset after an unforeseen discrepancy in vertical accuracy (Z) was observed in previous data collection efforts. The corrected GNSS+RTK achieved notably high vertical accuracy assessment Z (cm), as indicated by the low error values.

In conclusion, the results consistently highlight GNSS+RTK as the most effective georeferencing method among those tested, particularly in terms of its vertical accuracy. This finding has significant implications for precision agriculture applications such as plant height estimation from UAS imagery and reinforces the importance of choosing the appropriate georeferencing method for achieving accurate and reliable data.

5.1.2 Discussion

The two primary objectives of this study, georeferencing systems comparison and plant height estimation, encountered challenges due to the accuracy of the UAS imagery data and the survey of GCPs using GNSS+RTK and the EMLID RS2 receiver. This became evident when the original geospatial data — consisting of latitude, longitude, and ellipsoid height — was compared with the newly acquired geographical data derived from two different sources: OPUS processing services and TxDOT RTN. The comparison revealed that the ellipsoid height had been compromised by a height error of approximately 1.2 meters. Interestingly, both systems displayed a comparable level of error, which kept the measurements on a similar scale. However, a deeper investigation unearthed an additional discrepancy: the GNSS+RTK rod's height was offset by 1.802 meters.

Concerning the georeferencing systems comparison objective, the investigation was prompted by the high inaccuracy of the vertical accuracy assessment. Further analysis revealed that the overlooked height of the RTK collector above the ground, when operating the DJI D-RTK 2 base station, was a significant underlying factor. As the GNSS base station receiver's measurement is taken at the phase center in the antenna, a correction of subtracting 1.802 meters from the original point was necessary. Subsequent results, as demonstrated in the figure 5.23, indicated enhanced accuracy concerning the vertical accuracy assessment when using GNSS+RTK.

Results consistently showed that GNSS+RTK yielded the best outcomes across data collected on multiple dates (figures 5.13, 5.14, 5.15, 5.16, 5.18, 5.19, 5.20, 5.21). Furthermore, the use of one GCP improved accuracy compared to scenarios with no GCPs used, while GNSS-only without any GCP reported the least accurate results.

These findings underscore the critical role of rigorous georeferencing techniques, GCP utilization, and precise calibration of RTK systems for enhancing the reliability and accuracy of geospatial data in precision agriculture and remote sensing applications. This study thus provides a valuable reference for future research and applications in these fields.

5.2 Plant Height Estimation

5.2.1 Results

The estimation of plant height in the study was conducted through a robust comparison between manually measured plant height and the height obtained post-processing of datasets using the SfM algorithm. For this analysis, the georeferencing method used for imagery collection was GNSS+RTK. Further, during the SfM processing stage within PIX4Dmapper, a total of five GCPs were selected as 3D GCPs. This selection included one GCP at each corner of the field and one in the center to minimize the bowl effect in photogrammetry. The remaining four GCPs were designated as checkpoints.

A key metric in this analysis was the determination of the coefficient of determination (R^2) value, which provided a measure of how closely the estimated plant height matched the manually measured values, thereby offering a quantitative assessment of the accuracy of the approach. To further refine plant height estimation, three different methods were employed to create a DTM: DTM derived from automatic classification on PIX4Dmapper, DTM obtained by interpolating ground points, and DTM generated from flight conducted before plant emergence. Each of these methods offered distinct perspectives on the terrain and plant height, adding depth to the understanding of the subject. Additionally, the analysis accounted for variations in green canopy cover within defined plot boundaries. The results were examined systematically for different percentages of green canopy cover, highlighting the influence of vegetation density on plant height estimation.

In table 5.5 and figure 5.24, for data collected on the 1st of June, 2022, there was no significant difference from results when comparing DTM from interpolating ground points and DTM from before the plant emerged. Automatically classification of ground points for the creation of DTM performed slightly worse for boundaries with canopy cover higher than 90 percent, but better for most canopy cover scenario. In every scenario, canopy cover higher than 90 percent reported the most accurate results.

Table 5.5
Coefficient of determination (R^2) values obtained from various DTM creation techniques and different green canopy cover percentages for 06/01/2022.

Experiment Compared	**R^2**
DSM, DTM from Pix4DMapper Automatic Classification Tool for 36 plants	0.33
DSM, DTM from Pix4DMapper Automatic Classification Tool CC $\geq$ 60	0.27
DSM, DTM from Pix4DMapper Automatic Classification Tool CC $\geq$ 70	0.29
DSM, DTM from Pix4DMapper Automatic Classification Tool CC $\geq$ 90	0.89
DSM from Pix4DMapper – DTM Interpolated for 36 plants	0.30
DSM from Pix4DMapper – DTM Interpolated CC $\geq$ 60	0.25
DSM from Pix4DMapper – DTM Interpolated CC $\geq$ 70	0.27
DSM from Pix4DMapper – DTM Interpolated CC $\geq$ 80	0.73
DSM from Pix4DMapper – DTM Interpolated CC $\geq$ 90	0.92
DSM from Pix4DMapper – DTM from March 26th, 2022 flight for 36 plants	0.32
DSM from Pix4DMapper – DTM from March 26th, 2022 flight CC $\geq$ 60	0.27
DSM from Pix4DMapper – DTM from March 26th, 2022 flight CC $\geq$ 70	0.29
DSM from Pix4DMapper – DTM from March 26th, 2022 flight CC $\geq$ 80	0.70
DSM from Pix4DMapper – DTM from March 26th, 2022 flight CC $\geq$ 90	0.92

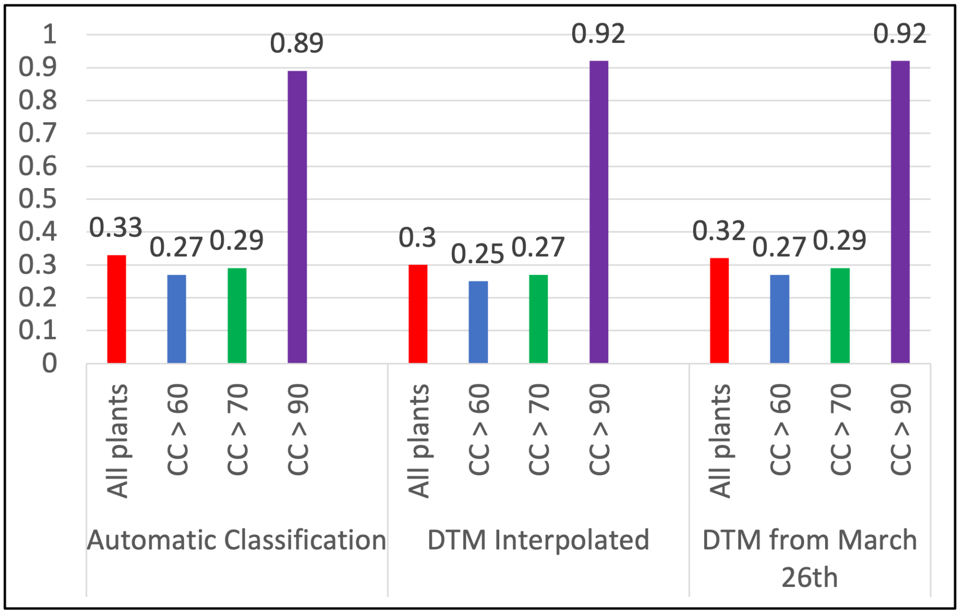

Figure 5.24
Coefficient of determination (R^2) values obtained from various DTM creation techniques and different green canopy cover percentages for 06/01/2022.

In table 5.6 and figure 5.25, for data collected on the 16th of June, 2022, DTM generated from interpolating ground points resulted in higher coefficient of determination (R^2). Automatically classification of ground points for the creation of DTM performed better than DTM obtained from flight conducted before plant emergence. In every scenario, canopy cover higher than 64 percent reported the most accurate results.

Table 5.6
Coefficient of determination (R^2) values obtained from various DTM creation techniques and different green canopy cover percentages for 06/16/2022.

Experiment Compared	**R^2**
DSM, DTM from Pix4DMapper Automatic Classification Tool for 36 plants	0.42
DSM, DTM from Pix4DMapper Automatic Classification Tool CC ≥ 60	0.53
DSM, DTM from Pix4DMapper Automatic Classification Tool CC ≥ 64	0.74
DSM from Pix4DMapper – DTM Interpolated for 36 plants	0.43
DSM from Pix4DMapper – DTM Interpolated CC ≥ 60	0.64
DSM from Pix4DMapper – DTM Interpolated CC ≥ 64	0.78
DSM from Pix4DMapper – DTM from March 26th, 2022 flight for 36 plants	0.38
DSM from Pix4DMapper – DTM from March 26th, 2022 flight CC ≥ 60	0.49
DSM from Pix4DMapper – DTM from March 26th, 2022 flight CC ≥ 64	0.62

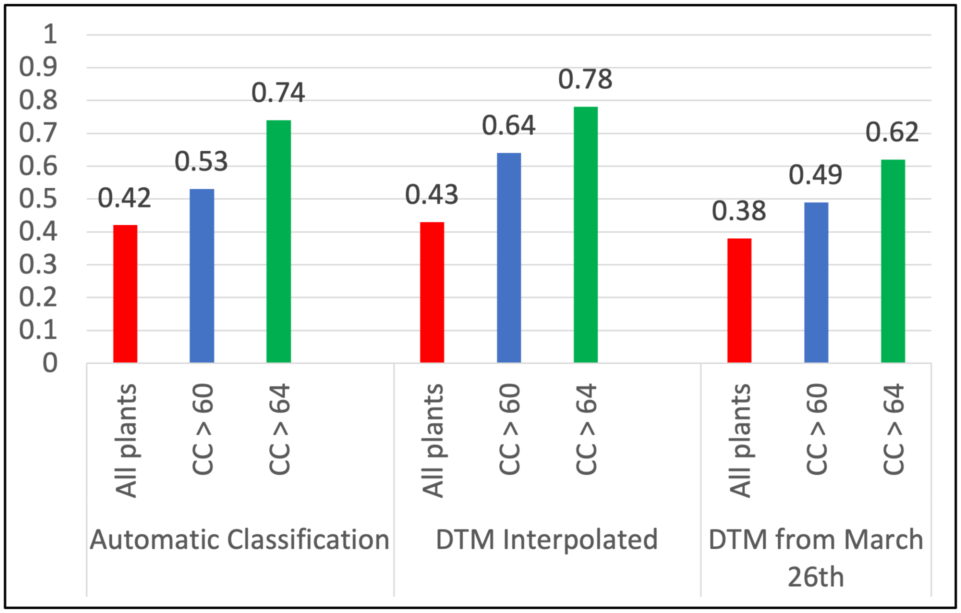

Figure 5.25
Coefficient of determination (R^2) values obtained from various DTM creation techniques and different green canopy cover percentages for 06/16/2022.

5.2.2 Discussion

In this study, the accuracy of plant height estimation was evaluated, an important aspect of precision agriculture. Manually measured plant height with height obtained through processing datasets with the SfM algorithm was compared. The accuracy was determined by the coefficient of determination (R^2) value, a measure of how close the estimated plant height matched the manual measurements.

Three unique methods were utilized for creating a DTM: automatic classification on PIX4Dmapper, interpolating ground points, and using pre-plant emergence flight data. The quality and accuracy of the plant height estimates were significantly influenced by the DSM, its resolution, and the quality of the 3D point cloud generated from the SfM/MVS workflow in PIX4Dmapper.

Our analysis considered variations in green canopy cover and examined results for different percentages. As shown in tables 5.5 and 5.6, high canopy cover percentages generally led to more accurate results. Moreover, it was found that factors such as plant color, possibly linked with maturity and health, could influence the accuracy of plant height estimation.

The comparison of different DTM creation methods showed slight differences. For data collected in June 1st, the DTMs generated from interpolated ground points and pre-plant emergence flights yielded similar results. On the other hand, for data collected in June 16th, the DTMs generated from interpolated ground points outperformed automatic classification and pre-plant emergence flights.

These findings emphasize the importance of multiple factors, including the DTM creation method, the percentage of green canopy cover, plant color and maturity, and the quality of the UAS-SfM generated DSM, in achieving accurate corn height estimations. Moreover, maintaining the same resolution in the DTM, DSM, and Canopy Height Model (CHM) contributes to the precision and reliability of the estimations.

Our study also showed potential for accurate early-season plant height estimations through precise georeferencing and GCPs utilization, with either GNSS+RTK or GNSS+RTN.

Additionally, all DTM generation techniques were accurate for corn plants in their early maturity stage, offering adaptability in precision agriculture. Observations on plant color and maturity impacting estimation accuracy provide new research opportunities, such as exploring different spectral bands to account for variations in plant color and maturity, enhancing plant height estimation.

However, there were limitations, including late flight timing introducing potential inaccuracies in phenotypic plant data, potential errors in input coordinates for the DJI D-RTK 2 Mobile Station (GNSS+RTK) and EMLID Reach base station impacting georeferencing accuracy, and flight parameters like wind conditions and grid missions affecting image quality.

In future research, scheduling flights at different crop maturity stages and ensuring accurate input coordinates, alongside methodological refinements like windless conditions and double grid missions, can enhance geospatial data quality. Flying at lower altitudes may also improve the point cloud quality. These adjustments can enhance georeferencing and plant height estimation methodologies, contributing to better precision agriculture practices.

CHAPTER 6: CONCLUSIONS & FUTURE WORK

6.1 Conclusions

The overarching goal of this research was to asses different georeferencing techniques and DTM generation method to improve geospatial data quality and crop canopy height estimation in the field of UAS-SfM surveying.

In our analysis comparing different georeferencing systems, it initially seemed that the GNSS+RTK method consistently outperformed the other techniques, delivering more accurate results across various dates. This was especially evident in the context of vertical accuracy, where it seemed to surpass the results of GNSS-only and GNSS+RTN methods. An impressive improvement was also seen in the accuracy of the ellipsoid height measurements when using GNSS+RTK, once the overlooked height of the RTK collector off the ground was corrected. This underlined the importance of careful setup and calibration in RTK systems for precise results. Also there was a remarkable improvement in accuracy when at least one GCP was used, compared to scenarios where no GCPs were employed. In contrast, the GNSS-only method, when used without any GCPs, tended to deliver the least accurate results in all our tests. These results emphasize the importance of using GCPs and the GNSS+RTK method to increase georeferencing accuracy. However, a note of caution must be added. Despite these overall trends, there were some instances where the GNSS+RTK method did not consistently outperform the other techniques. A notable example was the large error observed in the GNSS+RTN and 1 GCP Vertical accuracy (Z) for the data collected on 06/16/2022. This discrepancy was significantly larger than those seen on other dates, indicating some inconsistency in the results. This reminds us that while the GNSS+RTK method might generally deliver superior accuracy, there can be exceptions, and further investigation is required to understand these inconsistencies.

The importance of GCPs in the georeferencing process was a key finding in the study. It was revealed that even the inclusion of a single GCP could enhance the accuracy of results. This insight highlights the value of incorporating GCPs into georeferencing practices, underlining their role in shaping effective decision-making and management strategies in agriculture. Consequently, the findings from this study can contribute to the optimization of precision farming strategies and workflows, ultimately enhancing the overall efficiency and productivity of agricultural operations.

Comparing the DTM creation methods yielded insightful differences. For instance, in June 1st, the DTMs generated from interpolated ground points and pre-plant emergence flights yielded similar results. In June 16th, the DTMs generated from interpolated ground points outperformed automatic classification and pre-plant emergence flights.

In summary, this study suggests that plant height estimation accuracy consistently improves with higher canopy cover percentages, a combination of factors including DTM creation methods, precise georeferencing, use of GCPs, and consideration of plant color and maturity can contribute to accurate and efficient UAS-SfM surveys methodologies in precision agriculture.

6.2 Recommendations & Future Work

Building upon the outcomes of this research, there are promising directions for future exploration in precision agriculture. The timing of data collection flights could be further optimized to enhance the accuracy of plant height estimation. This could entail scheduling flights at different crop maturity stages, yielding a broader range of phenotypic data. In addition, alterations to flight parameters, such as conducting operations during no-wind conditions, utilizing Double Grid missions for enhanced data points, and experimenting with lower flight altitudes may improve the quality of the UAS-SfM data collected. Ensuring the precise accuracy of input coordinates for devices like DJI D-RTK 2 Mobile Station and EMLID Reach base station is also of crucial importance to enhance georeferencing accuracy.

Future investigations could examine the accuracy of plant height estimations in different types of crops, thus testing the findings' generalizability. Concurrently, the impact of plant color and maturity on estimation accuracy warrants further study. The physical marking of plot boundaries instead of using the EMLID Reach rover could minimize potential errors, making this an area for future research.

Finally, these findings' practical applications extend beyond plant height estimation, potentially including plant volume calculation, which could offer more detailed insights into plant growth and health. Integrating these methods with other remote sensing technologies, such as multispectral imaging, can facilitate the generation of comprehensive phenotypic data on crop health. The potential benefits of LiDAR data in creating accurate point clouds makes it a compelling field for further research. These findings and methodologies can significantly contribute to precision agriculture; they highlight the need for ongoing research to continue advancing this field.

REFERENCES

A., H. M., Mengjiao, Y., Luping, F., Awais, R., Bangyou, Z., Xianchun, X., ... Zhonghu, H. (2019). Accuracy assessment of plant height using an unmanned aerial vehicle for quantitative genomic analysis in bread wheat. *Plant methods*, *15*(1), 37-37.

Alfred, L., Lev, R., & Dmitry, T. (2015). *Gps satellite surveying fourth edition* (4th ed.). Wiley.

Ali, T. (2012, 01). Positioning with wide-area gnss networks: Concept and application. *Positioning*, *3*. doi: doi:10.4236/pos.2012.31001

Andrade-Sanchez, P., Gore, M. A., Heun, J. T., Thorp, K. R., Carmo-Silva, A. E., French, A. N., ... White, J. W. (2013). Development and evaluation of a field-based high-throughput phenotyping platform. *Functional Plant Biology*, *41*(1), 68–79.

Andrews, D. P., Bedford, J., & Bryan, P. G. (2013). A comparison of laser scanning and structure from motion as applied to the great barn at harmondsworth, uk. *The International Archives of the Photogrammetry, Remote Sensing and Spatial Information Sciences*, *40*, 31–36.

Barbedo, J. G. A. (2016). A review on the main challenges in automatic plant disease identification based on visible range images. *Biosystems engineering*, *144*, 52-60.

Barker, J., Zhang, N., Sharon, J., Steeves, R., Wang, X., Wei, Y., & Poland, J. (2016). Development of a field-based high-throughput mobile phenotyping platform. *Computers and Electronics in Agriculture*, *122*, 74-85. Retrieved from `https://www.sciencedirect.com/science/article/pii/S0168169916000223` doi: doi:https://doi.org/10.1016/j.compag.2016.01.017

Barrero Farfan, I. D., Murray, S. C., Labar, S., & Pietsch, D. (2013). A multi-environment trial analysis shows slight grain yield improvement in texas commercial maize. *Field Crops Research*, *149*, 167-176. Retrieved from `https://www.sciencedirect.com/science/article/pii/S0378429013001421` doi: doi:https://doi.org/10.1016/j.fcr.2013.04.017

Bendig, J., Bolten, A., & Bareth, G. (2013a, 12). Uav-based imaging for multi-temporal, very high resolution crop surface models to monitor crop growth variability. *Photogrammetrie - Fernerkundung - Geoinformation*, *2013*(6), 551-562. Retrieved from `http://dx.doi.org/10.1127/1432-8364/2013/0200` doi: doi:10.1127/1432-8364/2013/0200

Bendig, J., Bolten, A., & Bareth, G. (2013b, 12). Uav-based imaging for multi-temporal, very high resolution crop surface models to monitor crop growth variability. *Photogrammetrie - Fernerkundung - Geoinformation*, *2013*(6), 551-562. Retrieved from http://dx.doi.org/10.1127/1432-8364/2013/0200 doi: doi:10.1127/1432-8364/2013/0200

Bendig, J., Yu, K., Aasen, H., Bolten, A., Bennertz, S., Broscheit, J., ... Bareth, G. (2015a). Combining uav-based plant height from crop surface models, visible, and near infrared vegetation indices for biomass monitoring in barley. *International Journal of Applied Earth Observation and Geoinformation*, *39*, 79-87. Retrieved from https://www.sciencedirect.com/science/article/pii/S0303243415000446 doi: doi:https://doi.org/10.1016/j.jag.2015.02.012

Bendig, J., Yu, K., Aasen, H., Bolten, A., Bennertz, S., Broscheit, J., ... Bareth, G. (2015b). Combining uav-based plant height from crop surface models, visible, and near infrared vegetation indices for biomass monitoring in barley. *International Journal of Applied Earth Observation and Geoinformation*, *39*, 79-87. Retrieved from https://www.sciencedirect.com/science/article/pii/S0303243415000446 doi: doi:https://doi.org/10.1016/j.jag.2015.02.012

Bendig, J., Yu, K., Aasen, H., Bolten, A., Bennertz, S., Broscheit, J., ... Bareth, G. (2015c). Combining uav-based plant height from crop surface models, visible, and near infrared vegetation indices for biomass monitoring in barley. *International Journal of Applied Earth Observation and Geoinformation*, *39*, 79-87. Retrieved from https://www.sciencedirect.com/science/article/pii/S0303243415000446 doi: doi:https://doi.org/10.1016/j.jag.2015.02.012

Benjamin, A. R., O'Brien, D., Barnes, G., Wilkinson, B. E., & Volkmann, W. (2020). Improving data acquisition efficiency: Systematic accuracy evaluation of gnss-assisted aerial triangulation in uas operations. *Journal of surveying engineering*, *146*(1).

Berry, P., & Spink, J. (2012). Predicting yield losses caused by lodging in wheat. *Field Crops Research*, *137*, 19-26. Retrieved from https://www.sciencedirect.com/science/article/pii/S0378429012002493 doi: doi:https://doi.org/10.1016/j.fcr.2012.07.019

Carles, F.-P., Javier, A., Pau, C., C., A., & Luis, E. (2011, 09). Gnss-sdr: An open source tool for researchers and developers. In (Vol. 2).

Carolan, M. (2017). Publicising food: Big data, precision agriculture, and co-experimental techniques of addition. *Sociologia ruralis*, *57*(2), 135-154.

Chang, Y. K., Zaman, Q. U., Rehman, T. U., Farooque, A. A., Esau, T., & Jameel, M. W. (2017). A real-time ultrasonic system to measure wild blueberry plant height during harvesting. *Biosystems Engineering*, *157*, 35-44. Retrieved from `https://www.sciencedirect.com/science/article/pii/S1537511016304639` doi: doi:https://doi.org/10.1016/j.biosystemseng.2017.02.004

Chapman, A., & Wieczorek, J. (2020). *Georeferencing best practices*. doi: doi:10.15468/doc-gg7h-s853

Chapman, S. C., Merz, T., Chan, A., Jackway, P., Hrabar, S., Dreccer, M. F., ... Jimenez-Berni, J. (2014). Pheno-copter: A low-altitude, autonomous remote-sensing robotic helicopter for high-throughput field-based phenotyping. *Agronomy*, *4*(2), 279–301. Retrieved from `https://www.mdpi.com/2073-4395/4/2/279` doi: doi:10.3390/agronomy4020279

Dao, T. H. D., Alves, P., & Lachapelle, G. (2004). Performance evaluation of multiple reference station gps rtk for a medium scale network. *Journal of Global Positioning Systems*, *3*(1&2), 173-182.

Dardanelli, G., Maltese, A., Pipitone, C., Pisciotta, A., & Lo Brutto, M. (2021). Nrtk, ppp or static, that is the question. testing different positioning solutions for gnss survey. *Remote Sensing*, *13*(7), 1406.

Dinkov, D. (2023, 04). Accuracy assessment of high-resolution terrain data produced from uav images georeferenced with on-board ppk positioning. *Journal of the Bulgarian Geographical Society*, *48*, 43-53. doi: doi:10.3897/jbgs.e89878

Duan, T., Zheng, B., Guo, W., Ninomiya, S., Guo, Y., & Chapman, S. C. (2017). Life science research - plant biology; findings from university of queensland in the area of plant biology described (comparison of ground cover estimates from experiment plots in cotton, sorghum and sugarcane based on images and ortho-mosaics captured by uav). *Life science weekly.*.

Eitel, J. U., Magney, T. S., Vierling, L. A., Brown, T. T., & Huggins, D. R. (2014). Lidar based biomass and crop nitrogen estimates for rapid, non-destructive assessment of wheat nitrogen status. *Field Crops Research*, *159*, 21-32. Retrieved from `https://www.sciencedirect.com/science/article/pii/S0378429014000161` doi: doi:https://doi.org/10.1016/j.fcr.2014.01.008

Feng, A., Zhang, M., Sudduth, K. A., Vories, E., & Zhou, J. (2019). Cotton yield estimation from uav-based plant height. *Transactions of the ASABE*.

Feng, A., Zhou, J., Vories, E. D., Sudduth, K. A., & Zhang, M. (2020). Yield estimation in cotton using uav-based multi-sensor imagery. *Biosystems engineering*, *193*, 101-114.

Fountas, S., Carli, G., Sørensen, C. G., Tsiropoulos, Z., Cavalaris, C., Vatsanidou, A., ... Tisserye, B. (2015). Farm management information systems: Current situation and future perspectives. *Computers and electronics in agriculture*, *115*, 40-50.

Geipel, J., Link, J., & Claupein, W. (2014). Combined spectral and spatial modeling of corn yield based on aerial images and crop surface models acquired with an unmanned aircraft system. *Remote sensing (Basel, Switzerland)*, *6*(11), 10335-10355.

Grenzdörffer, G. J. (2014). Crop height determination with uas point clouds. *The International Archives of the Photogrammetry, Remote Sensing and Spatial Information Sciences*, *XL-1*, 135–140. Retrieved from `https://isprs-archives.copernicus.org/articles/XL-1/135/2014/` doi: doi:10.5194/isprsarchives-XL-1-135-2014

H., H. F., B., R. A., Adam, M., March, C., J., W. M., & J., H. M. (2016). High throughput field phenotyping of wheat plant height and growth rate in field plot trials using uav based remote sensing. *Remote Sensing*, *8*(12). Retrieved from `https://www.mdpi.com/2072-4292/8/12/1031` doi: doi:10.3390/rs8121031

Hammerle, M., & Hofle, B. (2016). Direct derivation of maize plant and crop height from low-cost time-of-flight camera measurements. *Plant methods*, *12*(1), 50-50.

Harwin, S., & Lucieer, A. (2012). Assessing the accuracy of georeferenced point clouds produced via multi-view stereopsis from unmanned aerial vehicle (uav) imagery. *Remote Sens-*

ing, *4*(6), 1573–1599. Retrieved from `https://www.mdpi.com/2072-4292/4/6/1573` doi: doi:10.3390/rs4061573

He, Y., Qiao, G., Li, H., Yuan, X., & Li, Y. (2021). Unmanned aerial vehicle derived 3d model evaluation based on icesat-2 for ice surface micro-topography analysis in east antarctica. *International archives of the photogrammetry, remote sensing and spatial information sciences.*, *XLIII-B3-2021*, 463-468.

Hu, G. R., Khoo, K., Goh, P. C., & Law, C. L. (2002). Internet-based gps vrs rtk positioning with a multiple reference station network. *Journal of global positioning systems*, *1*(2), 113-120.

Hu, P., Chapman, S. C., Wang, X., Potgieter, A., Duan, T., Jordan, D., ... Zheng, B. (2018). Estimation of plant height using a high throughput phenotyping platform based on unmanned aerial vehicle and self-calibration: Example for sorghum breeding. *European Journal of Agronomy*, *95*, 24-32. Retrieved from `https://www.sciencedirect.com/science/article/pii/S1161030118300509` doi: doi:https://doi.org/10.1016/j.eja.2018.02.004

Hütt, C., Bolten, A., Hüging, H., & Bareth, G. (2022, 12). Uav lidar metrics for monitoring crop height, biomass and nitrogen uptake: A case study on a winter wheat field trial. *PFG – Journal of Photogrammetry Remote Sensing and Geoinformation Science*, *91*. doi: doi:10.1007/s41064-022-00228-6

Javier, G., A., A. C. F., Jordi, G.-M., R., R.-P. J., & Eduard, G. (2020). Analyzing and overcoming the effects of gnss error on lidar based orchard parameters estimation. *Computers and electronics in agriculture*, *170*, 105255.

Jayathunga, S., Owari, T., & Tsuyuki, S. (2018). Evaluating the performance of photogrammetric products using fixed-wing uav imagery over a mixed conifer–broadleaf forest: Comparison with airborne laser scanning. *Remote Sensing*, *10*(2). Retrieved from `https://www.mdpi.com/2072-4292/10/2/187` doi: doi:10.3390/rs10020187

Kaloop, M. R., Yigit, C. O., El-Mowafy, A., Dindar, A. A., Bezcioglu, M., & Hu, J. W. (2020). Hybrid wavelet and principal component analyses approach for extracting dynamic motion characteristics from displacement series derived from multipath-affected high-rate gnss observations. *Remote sensing (Basel, Switzerland)*, *12*(1), 79.

Kefauver, S. C., Vicente, R., Vergara-Díaz, O., Fernandez-Gallego, J. A., Kerfal, S., Lopez, A., ... Araus, J. L. (2017). Comparative uav and field phenotyping to assess yield and nitrogen use efficiency in hybrid and conventional barley. *Frontiers in plant science*, *8*, 1733-1733.

Khan, Z., Chopin, J., Cai, J., Eichi, V.-R., Haefele, S., & Miklavcic, S. J. (2018). Quantitative estimation of wheat phenotyping traits using ground and aerial imagery. *Remote Sensing*, *10*(6). Retrieved from `https://www.mdpi.com/2072-4292/10/6/950` doi: doi:10.3390/rs10060950

Lee, K. J. Y., & Park, J. (2002). Enhancement of continuty and accuracy by gps/glonass combination, and software developmen. *Korean Journal of Geomatics*, *2*, 65-73.

Li, B., Xu, X., Zhang, L., Han, J., Bian, C., Li, G., ... Jin, L. (2020). Above-ground biomass estimation and yield prediction in potato by using uav-based rgb and hyperspectral imaging. *ISPRS Journal of Photogrammetry and Remote Sensing*, *162*, 161-172. Retrieved from `https://www.sciencedirect.com/science/article/pii/S0924271620300538` doi: doi:https://doi.org/10.1016/j.isprsjprs.2020.02.013

Li, W., Niu, Z., Chen, H., Li, D., Wu, M., & Zhao, W. (2016). Remote estimation of canopy height and aboveground biomass of maize using high-resolution stereo images from a low-cost unmanned aerial vehicle system. *Ecological Indicators*, *67*, 637-648. Retrieved from `https://www.sciencedirect.com/science/article/pii/S1470160X16301406` doi: doi:https://doi.org/10.1016/j.ecolind.2016.03.036

Liang, H., Guijun, Y., Huayang, D., Hao, Y., Bo, X., Haikuan, F., ... Xiaodong, Y. (2019). Fuzzy clustering of maize plant-height patterns using time series of uav remote-sensing images and variety traits. *Frontiers in plant science*, *10*, 926-926.

Llorens, J., Gil, E., Llop, J., & Escolà, A. (2011). Ultrasonic and lidar sensors for electronic canopy characterization in vineyards: Advances to improve pesticide application methods. *Sensors*, *11*(2), 2177–2194. Retrieved from `https://www.mdpi.com/1424-8220/11/2/2177` doi: doi:10.3390/s110202177

Maimaitijiang, M., Sagan, V., Sidike, P., Maimaitiyiming, M., Hartling, S., Peterson, K. T., ... Fritschi, F. B. (2019). Vegetation index weighted canopy volume model (cvmvi) for soybean biomass estimation from unmanned aerial system-based rgb imagery. *ISPRS Journal of Photogrammetry and Remote Sensing*, *151*, 27-41. Retrieved from `https://www.sciencedirect.com/science/article/pii/S0924271619300644` doi: doi:https://doi.org/10.1016/j.isprsjprs.2019.03.003

Malambo, L., Popescu, S., Murray, S., Putman, E., Pugh, N., Horne, D., ... Bishop, M. (2018). Multitemporal field-based plant height estimation using 3d point clouds generated from small unmanned aerial systems high-resolution imagery. *International Journal of Applied Earth Observation and Geoinformation*, *64*, 31-42. Retrieved from `https://www.sciencedirect.com/science/article/pii/S0303243417301800` doi: doi:https://doi.org/10.1016/j.jag.2017.08.014

Marcer, A., Haston, E., Groom, Q., Ariño, A. H., Chapman, A. D., Bakken, T., ... Wieczorek, J. R. (2021). Quality issues in georeferencing: From physical collections to digital data repositories for ecological research. *Diversity & distributions*, *27*(3), 564-567.

Marco, A., Thomas, P., Sanromà-Güixens, D., Jong-Hoon, W., A., S. A., Stöber, C., ... Bernd, E. (2001, 01). Performance evaluation of a multi-frequency gps/galileo/sbas software receiver. In (p. 2749-2761).

Mathews, A. (2021, 01). Structure from motion (sfm) workflow for processing drone imagery. In (p. 91-102).

Mathews, A. J., & Jensen, J. L. R. (2013). Visualizing and quantifying vineyard canopy lai using an unmanned aerial vehicle (uav) collected high density structure from motion point cloud. *Remote Sensing*, *5*(5), 2164–2183. Retrieved from `https://www.mdpi.com/2072-4292/5/5/2164` doi: doi:10.3390/rs5052164

Matteo, C., Umberto, R., & Giovanni, P. (2019, 10). Testing a gnss software receiver for end-user utilization..

Matteo, C., Umberto, R., & Giovanni, P. (2020, 02). Low-cost gnss software receiver performance assessment. *Geosciences*, *10*, 79. doi: doi:10.3390/geosciences10020079

Maurizio, F., Andrea, M., & Mario, N. (2009, 05). N–gene gnss receiver: Benefits of software radio in navigation..

Mora, O. E., Langford, M., Mislang, R., Josenhans, R., & Chen, J. (2022). Precision performance evaluation of rtk and rtn solutions: a case study. *Journal of spatial science*, *67*(3), 473-486.

Ouml, T., calan, & Tunalioglu, N. (2010). Data communication for real-time positioning and navigation in global navigation satellite systems (gnss)/continuously operating reference stations (cors) networks. *Scientific Research and Essays*, *5*, 2630-2639.

Paziewski, J. (2020). Recent advances and perspectives for positioning and applications with smartphone gnss observations. *Measurement science & technology*, *31*(9), 91001.

Petovello, M. G., O'Driscoll, C., Gérard, L., Daniele, B., & Murtaza, H. (2008). Architecture and benefits of an advanced gnss software receiver. *Journal of global positioning systems*, *7*(2), 156-168.

Regan, (2019). 'smart farming' in ireland: A risk perception study with key governance actors. *NJAS - Wageningen journal of life sciences*, *90-91*(1), 1-10.

Rovira-Garcia, A., Ibáñez-Segura, D., Orús-Perez, R., Juan, J. M., Sanz, J., & González-Casado, G. (2020). Assessing the quality of ionospheric models through gnss positioning error: methodology and results. *GPS solutions*, *24*(1).

S., N., & Mark, P. (2008, 01). Multichannel dual frequency glonass software receiver. *21st International Technical Meeting of the Satellite Division of the Institute of Navigation, ION GNSS 2008*, *2*.

Sankaran, S., Khot, L. R., Espinoza, C. Z., Jarolmasjed, S., Sathuvalli, V. R., Vandemark, G. J., . . . Pavek, M. J. (2015). Low-altitude, high-resolution aerial imaging systems for row and field crop phenotyping: A review. *European Journal of Agronomy*, *70*, 112-123. Retrieved from `https://www.sciencedirect.com/science/article/pii/S1161030115300095` doi: doi:https://doi.org/10.1016/j.eja.2015.07.004

Sanz-Ablanedo, E., Chandler, J. H., Rodríguez-Pérez, J. R., & Ordóñez, C. (2018). Accuracy of unmanned aerial vehicle (uav) and sfm photogrammetry survey as a function of the number and location of ground control points used. *Remote Sensing*, *10*(10). Retrieved from https://www.mdpi.com/2072-4292/10/10/1606 doi: doi:10.3390/rs10101606

Stanton, C., Starek, M. J., Elliott, N., Brewer, M., Maeda, M. M., & Chu, T. (2017). Unmanned aircraft system-derived crop height and normalized difference vegetation index metrics for sorghum yield and aphid stress assessment. *Journal of Applied Remote Sensing*, *11*(2), 026035. Retrieved from https://doi.org/10.1117/1.JRS.11.026035 doi: doi:10.1117/1.JRS.11.026035

Starek, M., & Wilkinson, B. (2022, 06). Aerial surveying technology. In (p. 341-392). doi: doi:10.1061/9780784416037.ch10

Sun, S., Li, C., & Paterson, A. H. (2017). In-field high-throughput phenotyping of cotton plant height using lidar. *Remote Sensing*, *9*(4). Retrieved from https://www.mdpi.com/2072-4292/9/4/377 doi: doi:10.3390/rs9040377

Tao, H., Feng, H., Xu, L., Miao, M., Yang, G., Yang, X., & Fan, L. (2020). Estimation of the yield and plant height of winter wheat using uav-based hyperspectral images. *Sensors*, *20*(4). Retrieved from https://www.mdpi.com/1424-8220/20/4/1231 doi: doi:10.3390/s20041231

Tattaris, M., Reynolds, M. P., & Chapman, S. C. (2016). A direct comparison of remote sensing approaches for high-throughput phenotyping in plant breeding. *Frontiers in plant science*, *7*, 1131-1131.

Tomaštík, J., Mokroš, M., Surovỳ, P., Grznárová, A., & Merganič, J. (2019). Uav rtk/ppk method—an optimal solution for mapping inaccessible forested areas? *Remote sensing*, *11*(6), 721.

Torres-Sánchez, J., López-Granados, F., Borra-Serrano, I., & Peña-Barragán, J. M. (2018, 02). Assessing uav-collected image overlap influence on computation time and digital surface model accuracy in olive orchards. *Precision Agriculture*, *19*, 115-133. doi: doi:10.1007/s11119-017-9502-0

Wallace, L., Lucieer, A., Watson, C., & Turner, D. (2012). Development of a uav-lidar system with application to forest inventory. *Remote sensing (Basel, Switzerland)*, *4*(6), 1519-1543.

Wang, K., & El-Mowafy, A. (2021). Effect of biases in integrity monitoring for rtk positioning. *Advances in Space Research*, *67*(12), 4025-4042. Retrieved from `https://www.sciencedirect.com/science/article/pii/S0273117721001794` doi: doi:https://doi.org/10.1016/j.asr.2021.02.032

Wang, X., Zhang, R., Song, W., Han, L., Liu, X., Sun, X., ... Zhao, J. (2019a). Dynamic plant height qtl revealed in maize through remote sensing phenotyping using a high-throughput unmanned aerial vehicle (uav). *Scientific reports*, *9*(1), 3458-3458.

Wang, X., Zhang, R., Song, W., Han, L., Liu, X., Sun, X., ... Zhao, J. (2019b). Dynamic plant height qtl revealed in maize through remote sensing phenotyping using a high-throughput unmanned aerial vehicle (uav). *Scientific reports*, *9*(1), 3458-3458.

Watanabe, K., Guo, W., Arai, K., Takanashi, H., Kajiya-Kanegae, H., Kobayashi, M., ... Iwata, H. (2017). High-throughput phenotyping of sorghum plant height using an unmanned aerial vehicle and its application to genomic prediction modeling. *Frontiers in plant science*, *8*, 421-421.

Westoby, M. J., Brasington, J., Glasser, N. F., Hambrey, M. J., & Reynolds, J. M. (2012). Structure-from-motion photogrammetry; a low cost, effective tool for geoscience applications. *Geomorphology (Amsterdam, Netherlands)*, *179*, 300-314.

Xie, C., & Yang, C. (2020). A review on plant high-throughput phenotyping traits using uav-based sensors. *Computers and Electronics in Agriculture*, *178*, 105731. Retrieved from `https://www.sciencedirect.com/science/article/pii/S0168169919320046` doi: doi:https://doi.org/10.1016/j.compag.2020.105731

Yilmaz, C. S., Yilmaz, V., & Güngör, O. (2018). Investigating the performances of commercial and non-commercial software for ground filtering of uav-based point clouds. *International Journal of Remote Sensing*, *39*(15-16), 5016-5042. Retrieved from `https://doi.org/10.1080/01431161.2017.1420942` doi: doi:10.1080/01431161.2017.1420942

Yuan, W., Li, J., Bhatta, M., Shi, Y., Baenziger, P. S., & Ge, Y. (2018). Wheat height estimation using lidar in comparison to ultrasonic sensor and uas. *Sensors*, *18*(11). Retrieved from `https://www.mdpi.com/1424-8220/18/11/3731` doi: doi:10.3390/s18113731

Yue, J., Yang, G., Li, C., Li, Z., Wang, Y., Feng, H., & Xu, B. (2017). Estimation of winter wheat above-ground biomass using unmanned aerial vehicle-based snapshot hyperspectral sensor and crop height improved models. *Remote Sensing*, *9*(7). Retrieved from `https://www.mdpi.com/2072-4292/9/7/708` doi: doi:10.3390/rs9070708

Zhang, Z., Liu, H., Yang, C., Ampatzidis, Y., Zhou, J., & Jiang, Y. (2022). *Unmanned aerial systems in precision agriculture*. doi: doi:10.1007/978-981-19-2027-1